Manuscript Details

Manuscript number	PSS_2019_141_R2
Title	In-Situ Approach for Thermal Energy Storage and Thermoelectricity generation on the Moon: Modelling and Simulation
Article type	Research Paper

Abstract

Human, tele-operated rovers, and surface infrastructures are now being actively considered for lunar polar exploration. Current approaches to energy provision consider, among others, hybrid direct energy/chemical technologies, such as solar photovoltaic arrays, batteries, and regenerative fuel cells. Due to the long period of darkness on the Moon and the challenges this poses to the aforementioned conventional energy generation and storage technologies, there is a need to assess the potential of In-Situ Resources Utilization (ISRU) methods to enable or supplement long duration missions. We present a computational model (MATLAB) of a Thermal Energy Storage (TES) system coupled to drive a heat engine (Thermoelectric Generator) to produce electricity. The TES medium designed is based off processed lunar regolith, an abundant material present on the surface of the Moon. The architecture has been optimized to provide a minimum electrical power of 36 W per unit after 66 hours of polar night, but the modular nature of the model allows other ranges of parameter to be simulated. A trade-off between this ISRU-based concept and conventional approaches for energy production and storage was performed and ranked TES and thermoelectricity generation as the least appropriate option. This result is valuable in a period of enthusiasm towards ISRU. It shows that processes exploiting extraterrestrial materials instead of Earth supplies are not systematically attractive. Despite the non-favorable performances for the proposed concept, some perspectives for the TES system are given as well as potential model improvements such as the need to assess the use of a Stirling heat engine.

Keywords	Thermal Energy Storage; Thermoelectric; MATLAB; Moon; ISRU

Corresponding Author	Patrick Fleith
Corresponding Author's Institution	European Space Agency
Order of Authors	Patrick Fleith, Aidan Cowley, Alberto Canals Pou, Aaron Valle Lozano, Rebecca Frank, Pablo Lopez Cordoba, Ricard González-Cinca
Suggested reviewers	Stéphanie Lizy-Destrez, Mario Fernández Palos, Victor Manuel Garcia, Cédric LE BOT

Submission Files Included in this PDF

File Name [File Type]

Final Revised Manuscript with changes marked.docx [Revised Manuscript with Changes Marked]

Highlights.docx [Highlights]

Final Manuscript.docx [Manuscript File]

declaration-of-competing-interests.docx [Conflict of Interest]

Submission Files Not Included in this PDF

File Name [File Type]

Final Responses To Reviewers.xlsx [Response to Reviewers]

Figure 1.png [Figure]

Figure 2.png [Figure]

Figure 3.png [Figure]

Figure 4a.png [Figure]

Figure 4b.png [Figure]

Figure 5a.png [Figure]

Figure 5b.png [Figure]

Figure 5c.png [Figure]

Figure 5d.png [Figure]

Figure 5e.png [Figure]

Figure 5f corrected.png [Figure]

To view all the submission files, including those not included in the PDF, click on the manuscript title on your EVISE Homepage, then click 'Download zip file'.

Research Data Related to this Submission

Data set	https://data.mendeley.com/datasets/bpnhbj34ch/draft?a=fda0e000-4bf7-458b-84cc-3f155fd911b7

Data for: In-Situ Approach for Thermal Energy Storage and Thermoelectricity generation on the Moon: Modelling and Simulation

1) Set stimulation settings and run the script 2) Tune Advanced Model and run the script 3) run save_results to save the results

In-Situ Approach for Thermal Energy Storage and Thermoelectricity generation on the Moon: Modelling and Simulation

Authors:

Patrick Fleith[ab*], Aidan Cowley[a], Alberto Canals Pou[ac], Aaron Valle Lozano[ade], Rebecca Frank[a], Pablo Lopez Cordoba[af], Ricard González-Cinca[f]

[a] *European Astronaut Centre (ESA/EAC), Linder Hoehe D-51147, Cologne, Germany*

[b] *ISAE-SUPAERO, 10 Avenue Edouard Belin, 31400 Toulouse, France*

[c] *Department of Materials Science and Metallurgy (CMEM), ETSEIB, Universitat Politècnica de Catalunya (UPC), Avda. Diagonal 647, 08028 Barcelona, Spain*

[d] *Luleå University of Technology, RYMDCAMPUS 1, 98192 Kiruna, Sweden*

[e] *Université Toulouse III - Paul Sabatier, Route de Narbonne, 31330 Toulouse, France*

[f] *Technical University of Catalonia-Barcelona Tech (UPC) c/ E. Terradas, 5. 08860 Castelldefels, Barcelona, Spain*

** Corresponding Author*

Abstract

Human, tele-operated rovers, and surface infrastructures are now being actively considered for lunar polar exploration. Current approaches to energy provision consider, among others, hybrid direct energy/chemical technologies, such as solar photovoltaic arrays, batteries, and regenerative fuel cells. Due to the long period of darkness on the Moon and the challenges this poses to the aforementioned conventional energy generation and storage technologies, there is a need to assess the potential of In-Situ Resources Utilization (ISRU) methods to enable or supplement long duration missions. We present a computational model (MATLAB) of a Thermal Energy Storage (TES) system coupled to drive a heat engine (Thermoelectric Generator) to produce electricity. The TES medium designed is based off processed lunar regolith, an abundant material present on the surface of the Moon. The architecture has been optimized to provide a minimum electrical power of 36 W per unit after 66 hours of polar night, but the modular nature of the model allows other ranges of parameter to be simulated. A trade-off between this ISRU-based concept and conventional approaches for energy production and storage was performed and ranked TES and thermoelectricity generation as the least appropriate option. This result is valuable in a period of enthusiasm towards ISRU. It shows that processes exploiting extraterrestrial materials instead of Earth supplies are not systematically attractive. Despite the non-favorable performances for the proposed concept, some perspectives for the TES system are given as well as potential model improvements such as the need to assess the use of a Stirling heat engine.

Keywords: Thermal Energy Storage; Thermoelectric; MATLAB; Moon; ISRU

Abbreviations:

- ESA: European Space Agency
- EVA: Extra-Vehicular Activity
- ISRU: In-Situ Resources Utilization
- ISS: International Space Station
- PDE: Partial Differential Equation
- SEC: Solar Energy Collector

- TC: Thermocouple
- TE: Thermoelectric
- TEG: Thermoelectric Generator
- TES: Thermal Energy Storage
- TM: Thermal Mass

1. Introduction

There is a renewed interest in returning astronauts to the Moon and establishing a sustainable human exploration capability on its surface. Indeed, the “Moon Village” concept was initiated by Jan Woerner, Director General of the European Space Agency (ESA), and is part of the vision of Space 4.0, a set of concrete actions for returning to the Moon in an environment for international cooperation and commercialization of space [1].

One of the greatest challenges in the exploration of the Moon, which is addressed from an ISRU perspective in this paper, is the storage of energy for missions involving lunar nighttime. Pragmatically, the rim of the Shackleton crater at the South Pole of the Moon is not only a key target of interest for science and exploration but it also allows substantial sun visibility [2], which reduces the potential complexity and mass of a stand-alone power system. Due to the prohibitive cost of transportation of materials from Earth, there is a need to assess In-Situ Resources Utilization (ISRU) approaches for energy production and storage. As ISRU has been identified as a key element to facilitate sustainable presence of humans in outer space (on the Moon or Mars), numerical modelling and simulation can enable us to assess its potential, and to compare it with other approaches. It is expected that through a smart use of ISRU, most of the systems could be built out of locally available resources, which would drastically decrease the amount of equipment launched from Earth. Nevertheless, the use of ISRU technologies has sometimes been questioned [3]. In this paper we propose and model a system for thermal energy storage in processed lunar regolith and electricity generation by means of thermoelectric converters. The advantages and disadvantages of the system with respect to other approaches have been analyzed in order to determine if the proposed concept has merit. The paper is organized as follows:

- Section 2 describes a realistic exploration scenario in the South Pole of the Moon, and its challenges in terms of energy production and storage. The variable sunlight conditions are addressed, and a plausible illumination profile is derived.
- An ISRU-based concept for Thermal Energy Storage on the Moon associated with Thermoelectric Generators (TES/TEG) is introduced in Section 3.

- Section 4 describes an integrated MATLAB model of the TES/TEG concept. The description includes the assumptions, data, and equations that have been used to build the model, such as temperature-dependent properties of regolith and thermoelectric materials.
- A trade-off analysis is presented in Section 5, in which the TES/TEG concept is compared to power subsystems based off solar arrays and batteries, solar arrays and regenerative fuel cells, and fission surface power. The trade-off analysis has ranked the TES/TEG concept as the least favorable alternative. It suggests that the concept and technologies need significant improvements to become more practically attractive. Therefore, a list of recommendations to improve the model and some general perspectives regarding ISRU-based thermal energy storage are provided in Section 6.

2. Exploration scenario of the Moon and the challenge of energy production and storage

2.1 Reasons for exploration of lunar South Pole

One of the major challenges for a long duration human surface mission will be provision of energy due to protracted darkness during the nighttime. The synodic period of the Moon is 29.54 days (709 hrs) [4]. At equatorial regions of the Moon, the lunar night can last up to 350 hours which is much longer than in the ISS (eclipses of 45 min). Therefore, the energy to be stored in order to meet a similar power demand would significantly increase on the Moon. In case batteries were used for energy storage, its number would be at least two orders of magnitude larger than in the ISS, which would lead to a dramatic increase of mass to be launched from Earth. Lunar poles are regions that benefit from long periods of sunlight due to the low elevation angle of the Sun and local topography [2]. Therefore, photovoltaic panels could be used for long periods, which would reduce the energy to be stored for the dark periods.

The polar temperature variations can be smaller at lunar poles (50°C) than at the equator (250°C) [5] which is an advantage for materials and infrastructures which are sensitive to degradation ~~sensitives to~~from high-amplitude thermal cycling [4]. However, the local topography and sun elevation at the poles could cause the number of thermal cycles to be greater than elsewhere on the Moon which affects planetary systems design.

Several lunar observation missions delivered ~~evidences~~evidence of the presence of water in the form of ice located in permanently shadowed regions near poles. Volatile water can be trapped in cold places such as these regions. The LCROSS mission estimated a mass concentration of water ice in the regolith of $5.6 \pm 2.9\%$ [6]. Water is of high importance to support human presence since drinkable water can be obtained from it, and O_2 and H_2 can be obtained by means of electrolysis.

The primary interest for lunar surface missions is the access to relevant terrains for science and exploration preparation, whereby geological, geophysical and geochemistry research can be performed and exploration enabling technologies can be demonstrated in-situ. In addition, the

aforementioned reasons for exploration of lunar South Pole are strong enablers for mission feasibility.

2.2 Determination of the illumination profile at the rim of the Shackleton crater

In order to study the potential of a solar-based concept for energy production and storage, it is necessary to identify the illumination profile at the target location. The South Pole presents some sites with high ~~level~~levels of sun visibility. These areas are located near the Shackleton crater, as depicted by the illumination map in Figure 1. They present high solar visibility, and a maximum continuous polar night significantly shorter than at equatorial regions.

In the considered scenario, any asset placed on the ~~Moon~~Moon's surface would experience a period of darkness between 100 and 250 hours maximum. However, two meters above the surface, the illumination conditions are much better. At a position of latitude -89.6866°N and longitude 197.19°E, the solar visibility is estimated to be 89.4% (over a 20-year period) and the maximum time continuously in shadow is 66 hours [2]. This illumination condition~~s~~ ~~represent~~represents therefore the best-case scenario (in term of longest darkness period) to study the feasibility of the concept. We assume that the solar energy collector would be mounted 2 m above the surface in order to increase solar visibility. This is possible since quantitative values are available from the literature as an input to our analysis [2]. One might argue that, instead, the worst illumination case scenario should be assessed. However, since the objective of this work is to determine if the proposed concept has merit, any negative assessment in the best-case scenario would also eliminate the choice of this power supply alternative for harsher conditions.

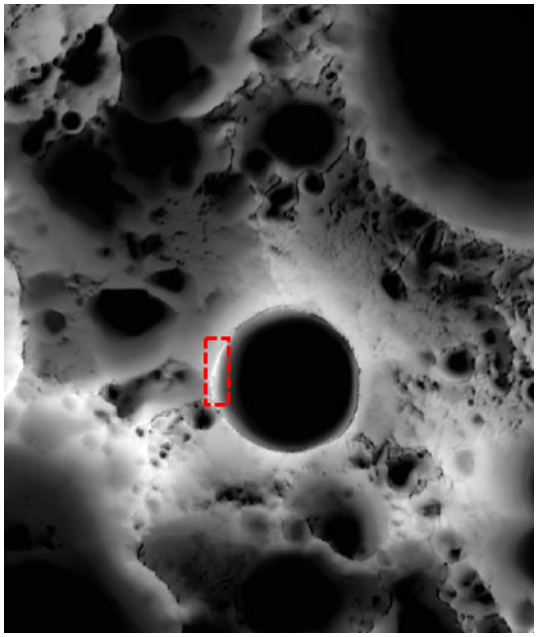

Figure 1: Multi-temporal illumination map of the lunar South Pole. The Shackleton crater (19 km diameter) is in the center. The South Pole is located approximately at 9 o'clock on its rim (highlighted region). Mapped area extends from 88°S to 90°S [7].

3. Thermal energy storage concept for electricity generation

An ISRU approach as a means of energy provision is to use the lunar regolith as the medium for thermal energy storage [8,9], similar to the underground thermal energy storage concept used on Earth. Heat can be stored in solid materials (thermal mass) in the form of sensible heat. A hot heat transfer fluid passes through the thermal mass heating it. If the heat losses are minimized, the thermal mass can be kept at high temperature, until the energy is released using the reverse mechanism. In this case, a cold working fluid passes through the thermal mass and absorbs the heat. The temperature of the fluid increases, which can be used as the source for a heating system.

The thermal masses can be fabricated at the Moon using sintered regolith. Sintering is accomplished by compacting loose material (powders, lunar dust) and forming a solid mass of material by applying heat and/or pressure. During this process, particles form strong bonds with a reduction in the volume of pores, with an attendant change in other material characteristics (e.g. bulk thermal conductivity). It has been demonstrated on Earth that lunar regolith simulant

can be processed into solid blocks (lunar bricks) with higher thermal conductivity than native regolith (by a factor 200). A 1.5 tons block made of lunar regolith simulant was 3D printed for proof of principle demonstration at the European Space Agency [10].

Figure 2 shows the proposed energy storage concept coupled with a heat engine. The concept is based on the thermal energy storage systems proposed in [8,9]. The system contains the following components: a solar energy concentrator to focus the incident sunlight and achieve a high heat flux; a thermal mass made of sintered regolith which is heated by the concentrated flux; a heat engine that converts the thermal energy into electricity, and a radiator that keeps the cold sink at low temperature. The different subsystems are described in the following modelling section.

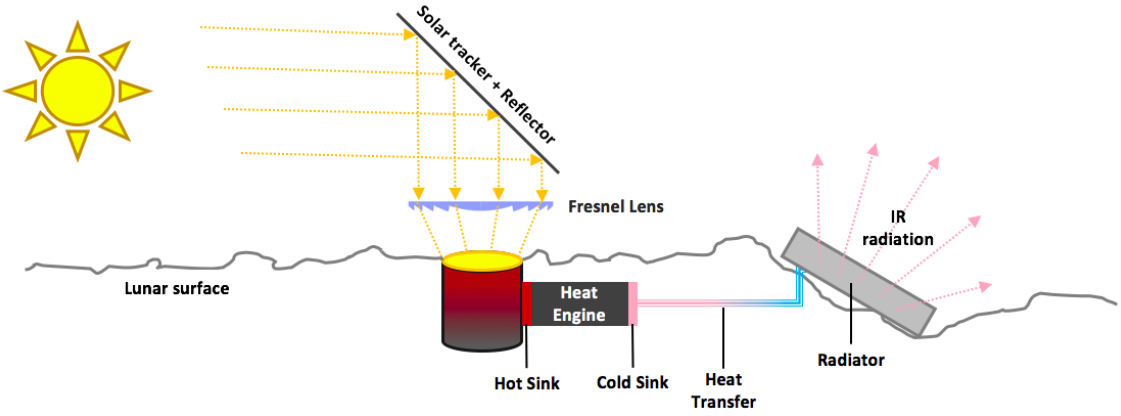

Figure 2: Thermal Energy Storage system coupled with a heat engine for electricity generation, and a radiator to cool down the cold sink.

4. Modelling the TES/TEG system

This section details the assumptions, data, and equations used to build the model for further assessment of the potential of the TES/TEG concept. The model has been implemented in MATLAB R2017b [11].

4.1 Modelling the solar energy collector

The objective of the Solar Energy Collector (SEC) is to collect and concentrate the solar flux to reach the high temperature desired for the thermal mass to store energy. The SEC is composed of a reflector and a concentrator. The reflector consists of a reflective mirror surface that can track the Sun position. The reflector is able to re-direct a high incidence flux perpendicularly to the target surface. Since a normal incidence flux is not sufficient, a Fresnel lens can be used to concentrate the Sun flux [12].

We assume that a reflector can ensure a minimum flux of $1000\ \mathrm{W.m^{-2}}$ during the polar day. This is acceptable given the general incoming solar flux on the Moon (neglecting ephemeris variations) is $\phi_{\mathrm{sun}} = 1365\ \mathrm{W.m^{-2}}$. The assumed lower value of the flux provided by the reflector accounts for efficiency of the mirrors (secular reflectivity estimated to be 85 to 90%), misalignments, actuation and geometrical limits. Thus, the heat flux given by the reflector is:

$$\phi_R = \begin{cases} 1000\ \mathrm{W.m^{-2}} & \text{(in sunlight)} \\ 0\ \mathrm{W.m^{-2}} & \text{(in shadow)} \end{cases} \qquad (1)$$

The concentrated flux of the SEC is given by:

$$\phi_C = f \cdot \eta_{FL} \cdot \phi_R\ , \qquad (2)$$

where f is the magnification of the Fresnel lens and η_{FL} its efficiency. With $f = 70$, a reflected flux of $1\ \mathrm{kW.m^{-2}}$ can be concentrated to achieve almost $70\ \mathrm{kW.m^{-2}}$. It is assumed that a magnification of $f = 70$ and only 5% of transmission losses can be achieved for a Fresnel lens optimized for the Moon. These assumptions are the basis for the concentrated solar flux and enable ~~to reach a~~the top surface temperature ~~for~~of the thermal mass ~~of~~to reach about 1000 K [13].

193

194 **4.2 Modelling the thermal mass**

195 The Thermal Mass (TM) thermally stores the energy and serves as a hot source for the heat
196 engine. It is made of sintered regolith and buried into the lunar native regolith to mitigate heat
197 losses. Indeed, the native regolith acts as insulator material, owing to its low thermal
198 conductivity. No loop heat pipes were considered inside the TM since its conductivity is already
199 enhanced with the sintering process. (average values of 2.1 $W.K^{-1}.m^{-1}$) for sintered regolith
200 against 0.01 $W.K^{-1}.m^{-1}$) for native regolith [14,15])

201 The model of the TM was implemented with the Partial Differential Equations (PDE) toolbox of
202 MATLAB. A 2D-model is chosen because a vertical cross-section of the entire TM is sufficient to
203 study the system. In previous studies, a cylindrical geometry of 0.5 m in height and 0.3 m in
204 diameter was considered [13,16]. These values are closely linked to manufacturing capability of
205 sintering methods. Because in this concept the TM is buried into lunar soil, automotive rovers or
206 astronauts would have to drill and excavate native regolith. The level of difficulty to perform this
207 operation for depths greater than 0.5 m – 1m is not well known. Sintering lunar rovers would
208 also have limited size. Therefore, the diameter is set to 0.3 m. These values were initially used
209 for the model and ultimately set to a depth of 0.65 m and width of 0.3 m for optimized
210 performances.

211 Figure 3 shows the designed TM buried into native regolith. At the top of the native regolith, a
212 'fluff' layer of regolith is modelled (with a very low thermal conductivity, see Table 1 and
213 Equation 7). On each side of the TM, an interface (hot sink plate) is modelled, and a hole is
214 defined within this geometry to model the presence of a TEG module. The overall model does
215 not have a meshed TEG since all computations for thermal transfers are done with a TEG
216 MATLAB function. We assume that the cold side of the TEG is connected to a cold plate which
217 rejects the heat through the radiator. Heat transfer from the TEG cold side to the radiator are
218 not implemented in this geometry since it is implemented in a separate function. Additionally, a
219 thermal conductance beam is modelled vertically in the middle of the TM in order to enhance
220 heat propagation through the medium. Although sintered regolith has a larger thermal

conductivity than fluff regolith, and thus a larger heat transfer rate, the optimization process of this work showed that the presence of a thermal beam substantially increases the system performance.

The PDE toolbox automatically generates the mesh and increases the number of nodes where it is needed (see Figure 3).

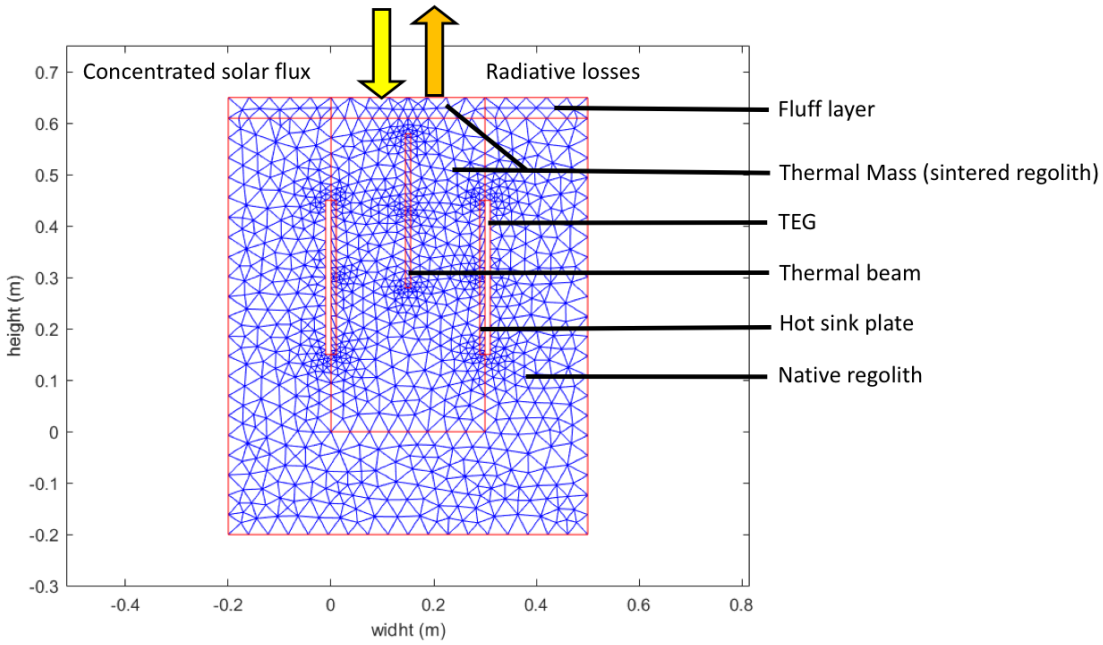

Figure 3: 2D-Model of the TM buried into lunar native regolith with a thermal beam in the middle and TEG modules on each side (white rectangles) attached to the hot sink plates. Note that the fluff layer does not extend on the top of the TM. The rectangle at the top of the TM is actually part of the sintered regolith block as pointed out on the figure.

The thermal mass model element can return the temperature at any time during the simulation as we solve a transient heat transfer problem with temperature dependent properties. The model accounts for heat gain from the Sun, losses, and energy extracted for power generation. The associated partial differential equation to be solved for conductive heat transfer is:

$$\rho \cdot c_p(T) \cdot \frac{\partial T}{\partial t} - \nabla \cdot (\kappa(T) \cdot \nabla T) = h, \quad (3)$$

where ρ is the density of the body, $c_p(T)$ its specific heat, T is the body's temperature, $\kappa(T)$ its thermal conductivity, and h is the heat generated inside the body. In order to solve Eq. 3, the

properties of sintered regolith, native regolith, and fluff layer are provided as inputs (Table 1). The surface emissivity of sintered regolith is assumed to be similar to native regolith emissivity. The surface absorptivity is assumed to be 0.85 since the Moon albedo ranges from 0.1 to 0.2 and the mean value for the surface of the Moon is 0.15 [17]. During the polar night, the surface emissivity of the TM is reduced by a factor 50 in order to account for radiative losses mitigation. This can be practically done by employing a highly reflective/insulating cover cap which covers the top of the TM during the polar night. This could be made with Multi-Layer Insulation (MLI) which has a high insulating performance (0.0006 $W.K^{-1}.m^{-1}$ for a 40-layer MLI) [3].

Table 1: Properties of native and fluff regolith. Sintered regolith properties are taken similar to basalt rock.

Properties	Native Regolith	Fluff layer	Sintered Regolith (basalt rock)
Density $(\mathrm{kg.m^{-3}})$	1800 [8]	1300 [18,19]	3000 [8]
Specific heat $(\mathrm{J.kg^{1}.K^{-1}})$	840-850 [8,14]	840-850 [8,14]	800 [8]
Thermal conductivity $(\mathrm{W.K^{-1}.m^{-1}})$	9.3×10^{-3} [8,14]	2.29×10^{-3} [18]	2.1 [8]
Surface emissivity $(-)$	0.96 [20]	0.96 [20]	0.96 [20]
Surface absorptivity $(-)$	0.85 [17]	0.85 [17]	0.85 [17]

It is important to implement the temperature dependence of the TM properties due to the large temperature variations. An expression for TM conductivity was obtained from a curve fit and interpolation of experimental data provided in the literature for the specific case of sintered lunar rock (resolidified) [14,21]:

$$\kappa_{TM}(T) = 6 \times 10^{-7} \cdot T^2 - 0.0028 \cdot T + 3.3753 \qquad (4)$$

Similarly the specific heat for lunar sintered regolith has been fitted to the following expression [14,22]:

$$c_{pTM}(T) = -5 \times 10^{-4} \cdot T^2 + 1.4332 \cdot T + 371.5 \qquad (5)$$

The native regolith conductivity [20,23]:

$$\kappa_{nat}(T) = 0.0093 \cdot \left\{1 + 0.073 \cdot \left(\frac{T}{350}\right)^3\right\} \quad (6)$$

The fluff regolith layer conductivity [20,24]:

$$\kappa_{fluff}(T) = 9.22 \times 10^{-4} \cdot \left\{1 + 1.48 \cdot \left(\frac{T}{350}\right)^3\right\} \quad (7)$$

Eqs. 3 to 7 and Table 1 are used to compute the conductive heat transfer between the thermal mass and the surrounding regolith. Convection mechanism are not considered since there is nearly vacuum on the Moon. The remaining losses are radiative heat losses, which are given by:

$$\phi_{rad} = \varepsilon_{TM} \cdot \sigma \cdot \left(T_{top}^4 - T_{space}^4\right), \quad (8)$$

where ϕ_{rad} is the radiative flux, ε_{TM} is the emissivity of the TM, σ is the Stefan-Boltzmann constant ($5.67 \times 10^{-8}\ \mathrm{W.m^{-2}K^{-4}}$), T_{top} is the temperature of the top surface of the TM facing outer space, T_{space} the temperature of deep space usually taken at 3 K. During the polar night $\varepsilon_{TM}(night)$ is taken as $\varepsilon_{TM}(day)/50$.

In order to compute the temperature in the TM, an initial temperature of the system has to be selected. 254 K is the bulk temperature beyond the thermal penetration depth of the lunar soil. The penetration depth usually ranges from 0.2 to 0.3 m. Therefore, the bottom boundary of the TM is set at a constant temperature of 254 K. To fix a constant temperature on a boundary, a *Dirichlet* boundary condition is employed in MATLAB.

The TM model also takes into account heat gain from the Sun flux and heat losses towards deep space (conduction losses are directly simulated by the model since native regolith surrounds the TM geometry). The TM receives a constant flux from the SEC during the polar day given by:

$$\phi_{SEC \to TM} = \alpha_{TM} \cdot \phi_C \quad (9)$$

$\alpha_{TM} = 0.85$ being the absorptivity of the TM.

The net flux absorbed by the element is given by $\phi_{SEC \to TM}$ and the radiation losses:

$$\phi_{net}(T) = \phi_{SEC \to TM} - \phi_{rad}(T) \quad (10)$$

$\phi_{net}(T)$ is set as a *Neumann* boundary condition in MATLAB at the top surface of the TM.

The general form of the partial differential equation solved by the MATLAB PDE Toolbox is:

$$m\frac{\partial^2 u}{\partial^2 t} + d\frac{\partial u}{\partial t} - \nabla \cdot (c\nabla u) + au = z, \quad (11)$$

Where in our model u corresponds to temperature and the coefficients are given by: $m = 0$, $d = \rho \cdot cp(T)$, $c = \kappa(T)$, and $z = h = 0$ (no heat generated in the system).

Unlike PDE's coefficients, *Neumann* boundary conditions cannot be set as temperature-dependent in the PDE toolbox of MATLAB. In order to overcome this problem, the simulation computes the temperature profile with a value of ϕ_{net} that is updated with the new temperature values at the end of each time step in the code. The time step was kept below 100 sec due to convergence issues if exceeding 120 sec.

4.3 Modelling the thermoelectric generator

The Thermoelectric Generator (TEG) ~~is connected to the~~ consists of an array of thermocouple materials assembled in series, sandwiched into two plates: one hot and one cold ~~plates.~~sink plates. The plates serve as interfaces between the thermoelectric array: on one side with the hot thermal mass, and on the cold side with the radiator where the wasted energy is dissipated (see Figure 2 and Figure 3). These plates are assumed to be a thin interface made of ~~ceramic or~~ conductive material in order to provide a homogeneous temperature for all thermocouples attached to it. Aluminum prevails in lunar regolith, mostly in form of oxides. Therefore, due to its high thermal conductivity and availability on-site, Aluminum was chosen as a good test candidate for the plates (see properties of Aluminum in Table 2). A conservative value for the thermal conductivity is taken to account for impurities and performance degradation due to thermal cycling.

Table 2: Properties of Aluminum used to model the hot and cold sink plates [25,26].

Properties	Hot/cold Sink Plate
Density (Al) $(\mathrm{kg.m^{-3}})$	2700
Specific heat (Al) $(\mathrm{J.kg^{-1}.K^{-1}})$	900
Thermal conductivity (Al) $(\mathrm{W.K^{-1}.m^{-1}})$	150
Thickness of plate (m)	0.01
Aluminum melting point (K)	932

306

307 The performance of a thermocouple depends on the working temperature, and the temperature
308 difference between the hot and cold plates. For this section, modelling strategies employed
309 previously [27–33] have been used.

310 The temperature difference between the hot and the cold plate ($\Delta T = T_h - T_c$) leads to the open
311 circuit voltage $V_{oc} = S(T_m) \cdot \Delta T$ due to the Seebeck effect given by

312 $$S(T_m) = |S_n(T_m)| + |S_p(T_m)|, \quad (12)$$

313 where $S(T_m)$ is the Seebeck coefficient, which depends on the mean temperature between the
314 hot and cold side, T_m . $S_n(T_m)$ and $S_p(T_m)$ are the Seebeck coefficients for the n-type and p-type
315 semiconductors, respectively. The value of $S(T_m)$ can be found in the literature and enables ~~to~~
316 ~~compute~~computation of the open circuit voltage:

317 Considering *n* thermocouples assembled in series, the open circuit voltage for the TEG is given
318 by $U_{oc} = n \cdot V_{oc}$.

319 Each thermocouple is made of one n-type and p-type leg with resistivity ρ_n and ρ_p , respectively,
320 which depend on the mean temperature. Therefore, the internal resistance of one thermocouple
321 is:

322 $$R_i = [\rho_n(T_m) + \rho_p(T_m)] \cdot \frac{h_{leg}}{A_{leg}}, \quad (13)$$

323 h_{leg} being the height of the leg (4.9 mm) and A_{leg} its area (2.5 mm * 2.5 mm) only for the case of
324 SiGe based thermocouples. Other thermocouples use a fixed resistance given in their

datasheets. The internal resistance for the TEG made of *n* thermocouples assembled in series is:

$$R_{i\,TEG} = n \cdot R_i \quad (14)$$

To maximize the power output from the TEG, the load resistance $R_{L\,TEG}$ (the resistance of the electrical system attached to the TEG) has to match the internal resistance, $R_{L\,TEG} = R_{i\,TEG}$. Thus, the load current I_L and voltage U_L are:

$$I_L = \frac{U_{oc}}{R_{i\,TEG} + R_{L\,TEG}} \quad (15)$$

$$U_L = U_{oc} - I_L \cdot R_{i\,TEG} \quad (16)$$

The output power provided by the TEG module is given by $P_{\text{elec}} = U_L \cdot I_L$.

Although the TEG module produces electricity out of the TM (hot source), one must consider that it also absorbs heat from it. This absorbed heat reduces the temperature of the TM during the polar night, which in turn decreases the temperature gradient across the TEG needed for electricity production. This negative retroactive effect has been considered in our study.

To obtain the relationships for the absorbed and rejected power in the TEG, three heat transfer mechanisms inside the thermocouple shall be considered. The Fourier process based on the material conductivity κ and the temperature difference ΔT between each side; the Joule heat dissipated due to current ~~flow~~flows I_L and internal electrical resistance R_i ; and the Peltier cooling/heat effect which is the phenomenon of heat absorption or dissipation at the junction of two dissimilar materials when an electrical current flow through this junction [28]. The heat absorbed or rejected based on the Peltier effect is given by $S(T) \cdot I_L \cdot T_{h\,\text{or}\,c}$. The combination of these three mechanisms for n thermocouples, gives the power absorbed at the hot side, and the power rejected at the cold side:

$$P_{abs} = n \cdot \left\{ -\frac{1}{2} \cdot R_i \cdot I_L^2 + S(T_m) \cdot I_L \cdot T_h + \kappa \cdot \Delta T \right\} \quad (17)$$

$$P_{rej} = n \cdot \left\{ \frac{1}{2} \cdot R_i \cdot I_L^2 + S(T_m) \cdot I_L \cdot T_c + \kappa \cdot \Delta T \right\} \quad (18)$$

The material thermal conductivity is often missing in TEG datasheet. However, it can be extracted from $\kappa = \frac{S(T_m)^2}{R_i \cdot Z}$, where $Z = \frac{ZT(T_{hot})Z_T(T_{hot})}{T_{hot} \quad T_{hot}}$, Z_T being the figure of merit. Therefore, the following parameters are required to compute all outputs: T_{hot}, T_{cold}, n, $ZT(T_{hot}Z_T(T_{hot}))$, R_i or R_i (T_m) and S or $S(T_m)$.

In the present case, three thermoelectric materials (Bi_2Te_3 [29], PbTe/TAGS [32], and SiGe [33]) have been considered and their properties are summarized in Table A.1 of Appendix A. The model of the TEG was implemented as a MATLAB function.

The TEG function was validated with the performance reported in the literature. The error in the simulated power output with respect to the datasheet is less than 2.5% for Bi_2Te_3 and PbTe/TAGS. For SiGe-based TEG, the simulated power output is within the uncertainty range presented in [33].

4.4 Modelling the cooling subsystem

The Cooling Subsystem (CS) works as follows: a cold plate absorbs the heat rejected by the thermoelectric generator, and the heat is evacuated to the radiator. As for the hot side, the chosen material is Aluminum. The temperature of the cold plate is computed as the temperature of the radiator assuming an ideal transfer of the TEG rejected heat. The chosen initial temperature in order to simulate the polar day is 250 K.

The radiator receives heat from the TEG and dissipates it towards the cold deep space. Thus, it is thermally coupled with space and the Moon's surface. Each contribution depends on the radiator geometry and orientation (view factors), the topography of the site, and the temperature profile of the lunar soil at that place. An ideal location for the radiator at the South Pole would be a permanent or long shadowed region. In this case, the radiator will achieve maximum performance due to the low environment temperature.

The radiator is assumed to be made of Aluminum. A coating surface is considered to maximize emitted heat flux, ε_{rad} , and minimize absorbed solar flux, α_{rad}. At beginning-of-life, common values for white epoxy materials are $\varepsilon_{rad} = 0.9$ and $\alpha_{rad} = 0.25$ [34]. However, due to solar high-energy radiation (UV), most of the ~~coating~~coatings age over time and, degraded sizing values

were used: $\varepsilon_{rad} = 0.8$ and $\alpha_{rad} = 0.4$. These values do not account for lunar dust depositing onto the radiator which could affect its overall emissivity and absorptivity.

The evolution of the temperature of the radiator is given by:

$$\frac{dT_{rad}}{dt} = \frac{1}{m_{rad}\, c_{prad}} \cdot \left(P_{rej} + P_{sun} - P_{radiator \to space} - P_{radiator \to moon}\right), \qquad (19)$$

where m_{rad} is the mass of the radiator, $c_{p_{rad}}$ is the specific heat of Aluminum, P_{sun} is the incoming power from the solar irradiance, $P_{radiator \to space}$ is the radiative power losses towards space, and $P_{radiator \to moon}$ is the net power transferred to the Moon surface. This latter contribution is assumed to be negligible, due to temperature equilibrium between the radiator placed directly on the fluff insulating regolith, and the possibility of carefully selection of the coating material. P_{sun} is given by:

$$P_{sun} = A_{rad} \alpha_{rad} \phi_{sun}, \qquad (20)$$

A_{rad} being the area of the radiator, α_{rad} the absorptivity of the coating, and ϕ_{sun} the direct sun irradiance. On the poles the maximum sun elevation is about 1.54° which would lead to an irradiance of $37\ \mathrm{W.m^{-2}}$. However, direct solar irradiance has been taken $100\ \mathrm{W.m^{-2}}$ as a worst-case value. This is to account for non-flatness of the local terrain which could cause the maximum sun elevation with respect to the radiator plane to be higher than expected at the poles. The radiator size needed is about 10 m².

The radiative power loss to space is given by:

$$P_{radiator \to space} = f_{rs} A_{rad} \varepsilon_{rad} \sigma \left({T_{rad}}^4 - {T_{space}}^4\right), \qquad (21)$$

where f_{rs} is the view factor considered equal to one (radiator placed horizontally on the lunar surface).

The change in temperature of the radiator (and thus the cold side) in a simulation time step Δt is finally given by:

$$\Delta T_{cold} = \Delta T_{rad} = \frac{1}{m_{rad}\, c_{prad}} \cdot \left(P_{rej} + P_{sun} - P_{radiator \to space}\right) \cdot \Delta t \qquad (22)$$

400

5. Results and Discussion

5.1 Performances optimizations and results

For the proposed TES/TEG concept, the main performance drivers have been identified through a fractional factorial design. Preliminary simulations have shown that the temperature experienced by the TEG at the hot sink is close to 410 K at the end of the polar night. Given this specific temperature differential (240 K) between the hot and cold plates and the cold plate temperature at the end of the darkness period (170 K), Bi_2Te_3 shows an efficiency (9.3%) higher than PbTe/TAGS (<9%) or SiGe (<3%). Bi_2Te_3 is the most obvious suitable material unless further materials are implemented in the model. It is worth mentioning that in the case of Bi_2Te_3, temperature-dependent properties were not available from the datasheet. However, due to the modularity of our model, it can be added in the future for better accuracy of results.

The influence of seven factors on the performance of the system was analyzed. The following four factors showed a significant influence:

- The power output of a TES/TEG unit at the end of a polar night is improved when the height of the TM it is set at 0.65 m rather than at 1 m.
- The ability of the cover cap to mitigate radiative losses. The model gave much better performance with a TM emissivity reduced by a factor 50 than with a TM emissivity reduced only by a factor 10 during the polar night.
- The achievable cold temperature plays an important role: 170 K at the cold side instead of 200 K significantly increases the power output.
- The presence of a thermal beam inside the TM substantially improved the system performance. Optimization of the dimension and location of this beam for better performances is left for future works. It is currently a preliminary design which gives a good compromise between performances improvement and mass of the thermal beam.

Other studied factors which had a negligible influence are:

- The surface occupied by the TEG (0.2 or 0.3 m^2), which impacts the absorbed heat flux.

- The depth at which the TEG is placed in the TM (0.2 or 0.3 m from the TM surface).
- The number of thermocouples per TEG (50 or 80).

Thanks to the identification of the main performance drivers, an ultimate simulation is performed which leads to the best performance of the system in the considered scenario. The numerical simulations reproduced the behavior of the system during 150 hours of concentrated sunlight followed by 66 hours of darkness. The results are presented in Fig. 4 and Fig. 5.

A steady temperature is reached at the end of the polar day (Figs. 4a and 5a). The top of the thermal mass reaches 1000 K while the bottom temperature stays at 600 K. This persistent gradient is explained by the relatively low thermal conductivity of sintered regolith, the heat absorbed by the TEG and the losses by conduction in native regolith.

At the end of the 66 hours of polar night, the temperature in the TM is more homogeneous and decreases to about 420 K (Figs. 4b and 5a). The coldest spots are the regions near the TEGs (Fig. 4b), since each TEG plate absorbs between 200 W and 400 W from the TM (Fig. 5d).

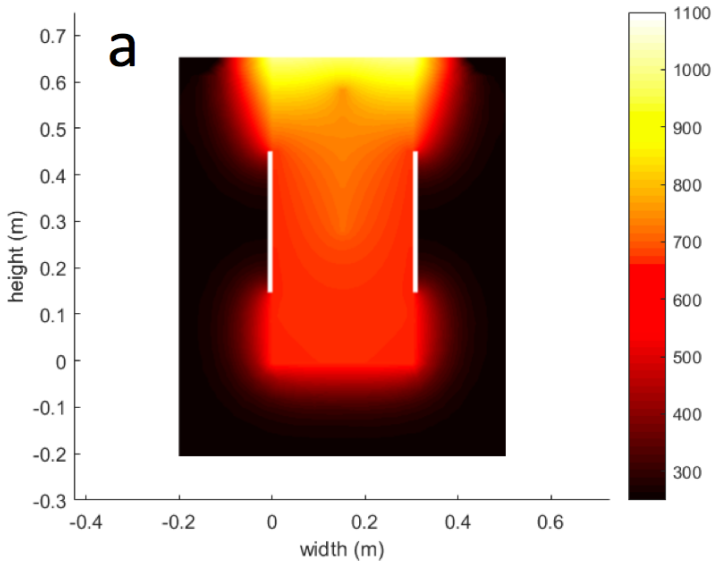

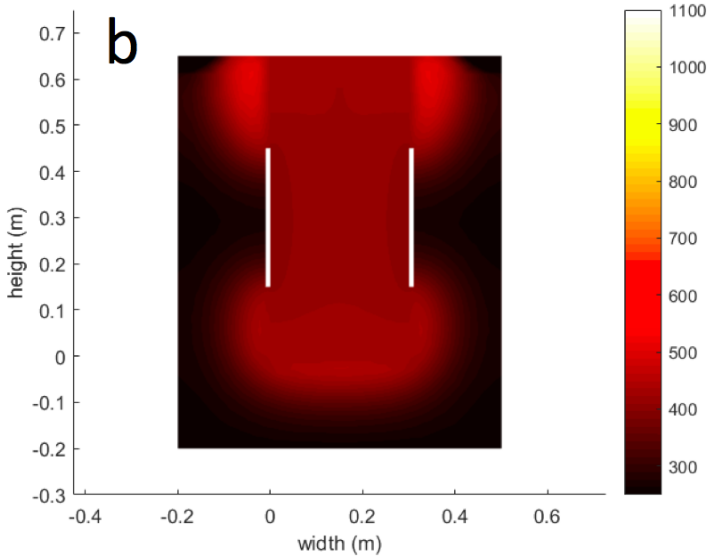

442

443 **Figure 4:** Temperature profile (K) of the thermal mass (a) after 150 hours of applied
444 concentrated sunlight (b) after 66 hours of radiative losses in the polar night. White rectangles
445 are the TEG modules.

446 The temperature difference achieved between the hot and the cold plates ranges from 240 K to
447 400 K (Fig. 5b). The peak observed after sunset is due to the sudden decrease of the cold plate
448 temperature. This peak in turn results in a peak in the power output (Fig. 5c), the heat flow
449 through each TEG element (Fig. 5d), and the efficiency of the TEG elements (Fig. 5e). The
450 efficiency of the TEG is within the range of expected values for thermoelectric materials (8 % to
451 11 %).

452 Similar to the TM temperature, the power output reaches a constant value during the polar day
453 at approximately 42 W per TEG (Fig. 5c) and sharply decreases during the polar night. At the
454 end of the darkness period, only 18 W are produced per TEG. Hence, the proposed concept
455 which includes two TEG plates provides a minimum of 36 W at any time during the 66 hours of
456 darkness considered.

457 Fig. 5f shows the number of required elements to provide 10 kW to a surface payload with a
458 very conservative 50% margin (accounting for a safety factor and low TRL technology). At the
459 end of the polar night, approximately 420 elements are needed to provide the required power.

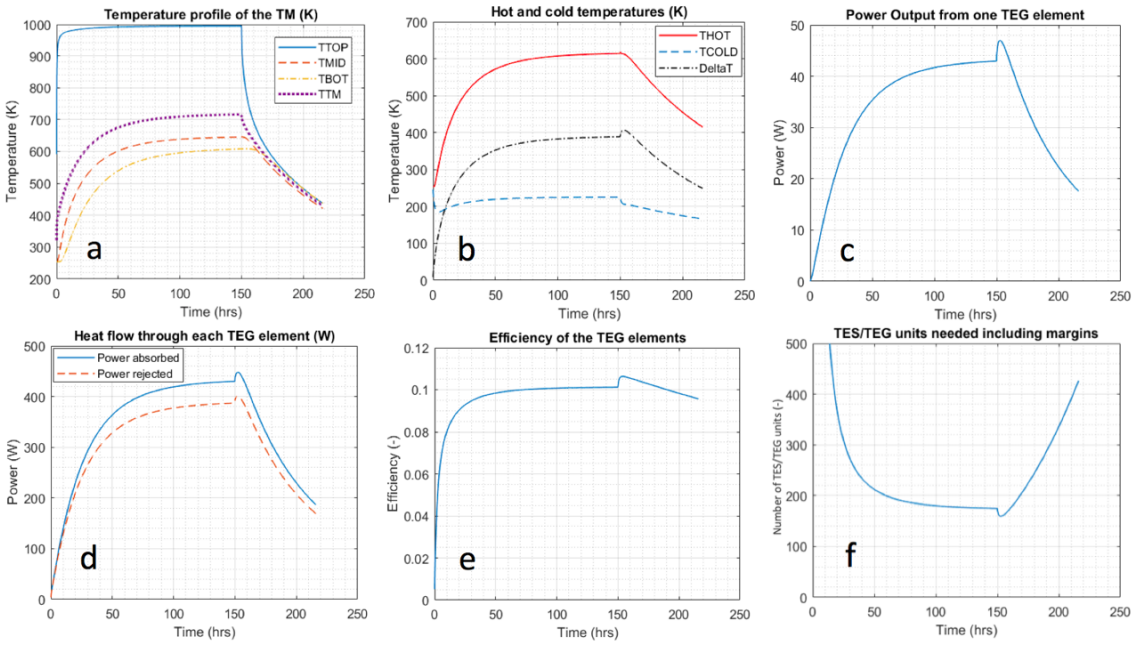

460

461 **Figure 5:** (a) temperature profile of the TM at the top (TTOP), mid-height (TMID), bottom
462 (TBOT), and mean value (TTM). (b) Temperature difference between the hot and cold plates (c)
463 Power output of one TEG (d) Power absorbed and rejected at the hot and cold plate,
464 respectively. (e) Efficiency of the TEG elements. f) Number of TES/TEG elements needed
465 including 50% to comply with 10 kW power requirement of a Moon base.

466 **5.2 Trade-off Analysis**

467 Trade-off analyses are frequently used to evaluate the potential of various alternatives, in order
468 to support a decision-making process. In the present case, the philosophy is to use it as a tool
469 to assess objectively the potential of our scenario concept with respect to more conventional
470 approaches. The analyzed systems are:

471 1) The TES/TEG system modelled in the present study.

472 2) A combination of solar panels and rechargeable batteries. This is the current approach used
473 on-board the ISS and by most of space missions in the vicinity of the Earth.

474 3) A combination of solar panels and regenerative fuel cells. This is a promising system since
475 fuel cells benefit from significant space heritage.

4) Fission Surface Power. An important advantage of this system is the continuous power production irrespective of the irradiance conditions, with a relatively compact system.

The trade-off analysis was performed considering the following criteria:

- **Mass of the power system:** Launch costs represent a significant part of any mission, and therefore a low-mass system is desirable given a fixed power requirement.
- **Global specific power**: Power output per unit of mass for the system. It is denoted as "global" since it is computed considering the global energy system mass (i.e. production units, storage mean, resources extracted from the Moon, structural elements, etc.). This criterion enables to assess the "compactness" of the system on the Moon.
- **Space heritage**: A space-proven technology is more likely to be used than a technology which requires years and considerable investment in research and technology development. The space heritage can be assessed using the technology readiness level scale (TRL)**.**
- **System complexity:** All characteristics being equal, a simple system is a better solution than a complex system. Indeed, knowledge acquisition is easier, and more confidence is placed during operations and maintenance. Furthermore, the end users would be able to interact easily, modify and adapt the system depending on real on-site situations.
- **Installation efforts:** This criterion aims to quantify the level of efforts that needs to be placed into the installation in the energy system before being operational. Some systems may be ready to use, mechanically deployable, or "plug & play". Some others might require robotic assisted installation, extensive ISRU, or extra-vehicular activities (EVAs) on the Moon surface.
- **Operations:** This criterion encompasses daily work required for astronauts, robots, ground control center, but also maintenance of the system. Safety issues due to hazardous components will also complicate operations, maintenance or work nearby the system.
- **Scalability:** The power system not only aims to provide electrical power to the primary habitat, but might be used for surface robots, pressurized rovers, EVA systems.

Moreover, new infrastructures will be progressively implemented and added to the main base in the “Moon Village”. Thus, it is important for a power system to be versatile, to interface with all of these elements, and to be scalable for increasing or decreasing power demand.

- **Lifespan:** For a long-duration program, the lifetime of the considered system should be high. Although no missions are yet fully planned, it is assumed that the return of humans to the ~~Moon~~Moon’s surface will be permanent, as it was for the Low-Earth Orbit. With unknown duration set, it is better to promote long lifespan systems, to account for permanent presence from program starting date.
- **Potential benefits for Earth systems:** Innovation and challenges encountered by engineers, scientist and astronauts often lead to advances beyond the limits of our technologies potentially leading to spin-off Earth applications.
- **End-Of-Life:** This criterion aims to assess potential constraints due to end-of-life management of the system, decommissioning, and recyclability for other uses.

Each technology has been assessed with respect to the criteria. The detailed scoring rules, the criteria weights, their evaluation and justification are available in Appendix B. Table 3 shows the synthesis trade-off matrix.

Table 3: Synthesis of the trade-off matrix for comparison of the performances of four energy production and storage systems at the rim of the Shackleton Crater (66 hours of polar night): Good (++); Medium (+); Bad (-); Very Bad (x). Baseline requirement is a power demand of 10kW.

Criteria/Systems	Solar Panels & Batteries	Solar Panels & Fuel Cells	Fission Surface	Thermal Energy Storage
Mass to be delivered from Earth	-	+	+ +	x
Specific Power	-	+	+ +	x
Space Heritage	+ +	+ +	+	-
System Complexity	+ +	-	x	+
Installation Efforts on the Moon	+ +	+	+	x
Operations	+ +	+ +	-	+ +
Scalability (up and down)	+ +	+	+	-
Lifespan	+	+	-	+ +
Potential benefit for Earth energy	+	+ +	-	+
End-of-life (recyclability, constraints?)	-	-	x	+
Total Figure of Merit	**85**	**80**	**46**	**28**

According to the results of the trade-off analysis, the use of a TES/TEG system to power the lunar base for 66 hours of darkness is not favorable with respect to other approaches. This negative result assessment is reinforced by the fact that the results were obtained in the best-case scenario, which is the unique spot of the Moon suspected to provide polar night as short as 66 hours [2]. This implies that such architecture would be much less able in harsher conditions. The main drawbacks in comparison with the alternative “Solar panels and Batteries” and “Solar panels and Regenerative Fuel Cells” are:

- Need of significant mass to be transported from Earth although ISRU activities take place (reflectors, Fresnel lens, TEG, aluminum plates, radiators). We estimated the delivered mass for one TES/TEG unit at 198 kg (see mass budget in appendix table B.2). Since it is computed that 420 units are required, the mass to be delivered to the Moon surface is about 82 tons for 10 kW of power demand. This is greater than for all other alternatives by almost a factor 5.
- Huge efforts necessary for installation. The total mass of regolith to be sintered on the Moon has been estimated to be about 245 metric tons. In addition, all the enabling systems to deploy the TES/TEG power architecture on the Moon were not considered

(comprising excavation, sintering, and connections of more than 420 TES/TEG units) which would add in reality considerable labor, costs, complexity and energy consumption for sintering.

- Lack of space heritage.

Despite the poor performance of the TES/TEG concept for the considered power requirement (10 kW), the outcome of this study is valuable because it shows that ISRU-based processes are not systematically advantageous against scenarios of Earth supplies.

6. Conclusions and future work

An integrated model of the TES/TEG concept has been presented in this paper. One major feature is the ability of the model to account for temperature dependent properties of the TM and TEG which was not the case in previous studies. The proposed system employs a TM of $1\ \mathrm{m} \times 0.3\ \mathrm{m} \times 0.65\ \mathrm{m}$ and Bi_2Te_3 thermoelectric generators. The system has been optimized to reach 36 W at the end of the 66 hours of the considered polar night 2 m above the surface at the rim of the Shackleton crater.

A trade-off analysis has been conducted in order to compare the TES/TEG concept with other architectures (solar arrays and batteries, solar arrays and regenerative fuel cells, fission surface power). The trade-off ranked the proposed TES/TEG system with thermoelectricity generation as the least appropriate alternative.

This result obtained under the best-condition scenario is valuable in a period of enthusiasm towards ISRU. It shows that processes exploiting extraterrestrial materials instead of Earth supplies are not systematically attractive. In actual fact, detailed analyses are required to verify if it has merit. Likewise, the ineffectiveness of thermoelectricity suggested in this specific case, should not preclude the use of thermal energy storage in a different architecture, or for other usages and scenarios.

Therefore, a number of follow-on considerations could also be studied which would open up the idea of ISRU TES systems in a more practical application:

- Integration of more efficient heat engines (TEGs with higher efficiencies, or a Stirling engine, which has a conversion efficiency of 25 to 30%) [9].
- Changing the location of the TEG on the TM appears very promising. We suggest replacing the TM cover cap by a TEG array which can be moved to be in contact with the top surface of the TM. During the polar day, the TEG array is not in contact with the surface that accumulates solar energy. During the darkness period, the TEG array is retracted and placed in contact with this hot surface. The advantage is that this surface is the hottest spot at the beginning of the nighttime, it prevents radiative losses and the need of a cover cap. This approach also reduces the need of a cooling system (including potential loop heat pipes) since the cold side area radiates directly the wasted energy towards deep space. The main drawback is the need for another power system during the polar day but this can be easily overcome with high-efficiency photovoltaic panels.
- Use of a TES/TEG only as a reliable power backup system instead of a primary power supply system, or only for thermal management purposes (thermal energy reservoir as part of a thermal Wadi concept) [15,35].
- Modelling of a single large power Thermal Energy Storage system: a 10-kW engine, and a large-scale TM with internal fluid loop heat pipes to enhance heat transfer for storage and release [9].

References

[1] ESA, Moon Village, (2016). http://www.esa.int/About_Us/Ministerial_Council_2016/Moon_Village (accessed April 15, 2019).

[2] P. Gläser, J. Oberst, G.A. Neumann, E. Mazarico, E.J. Speyerer, M.S. Robinson, Illumination conditions at the lunar poles: Implications for future exploration, Planet. Space Sci. (2017) 1–9. doi:10.1016/j.pss.2017.07.006.

[3] D. Rapp, Use of Extraterrestrial Resources for Human Space Missions to Moon or Mars, Springer, 2013. doi:10.1007/978-3-642-32762-9.

[4] D. Shrunk, B. Sharpe, B. Cooper, M. Thangavelu, THE MOON: Resources, Future Development, and Settlement, Second, Praxis Publishing Ltd, 2008.

[5] D.A. Paige, M.C. Foote, B.T. Greenhagen, J.T. Schofield, S. Calcutt, A.R. Vasavada, D.J. Preston, F.W. Taylor, C.C. Allen, K.J. Snook, B.M. Jakosky, B.C. Murrary, L.A. Soderblom, B. Jau, S. Loring, J. Bulharowski, N.E. Bowles, I.R. Thomas, M.T. Sullivan, C. Avis, E.M. De Jong, W. Hartford, D.J. McClesse, The Lunar Reconnaissance Orbiter Diviner Lunar Radiometer Experiment, Sp. Sci Rev. (2010) 125–160. doi:10.1007/s11214-009-9529-2.

[6] A. Colaprete, P. Schultz, J. Heldmann, D. Wooden, M. Shirley, K. Ennico, B. Hermalyn, W. Marshall, A. Ricco, R.C. Elphic, D. Goldstein, D. Summy, G.D. Bart, E. Asphaug, D. Korycansky, D. Landis, L. Sollitt, Detection of Water in the LCROSS Ejecta Plume, Science (80-.). 330 (6003) (2010) 463–468. doi:10.1126/science.1186986.

[7] NASA/GSFC, Multi-temporal illumination map of the lunar south pole, (2010). https://www.nasa.gov/mission_pages/LRO/multimedia/gallery/121510pole.html (accessed April 15, 2019).

[8] R. Balasubramaniam, R. Wegeng, S. Gokoglu, N. Suzuki, K. Sacksteder, Analysis of Solar-Heated Thermal Wadis to Support Extended-Duration Lunar Exploration, in: AIAA-

2009-1339, 2010.

[9] B. Climent, O. Torroba, R. González-cinca, N. Ramachandran, M.D. Griffin, Heat storage and electricity generation in the Moon during the lunar night, Acta Astronaut. 93 (2014) 352–358. doi:10.1016/j.actaastro.2013.07.024.

[10] ESA, Buidling a Lunar Base With 3D Printing, (2010). http://www.esa.int/Our_Activities/Space_Engineering_Technology/Building_a_lunar_base_with_3D_printing (accessed April 15, 2019).

[11] P. Fleith, In-Situ Approaches for Thermal Energy Storage and Thermoelectricity Generation on the Moon: Modelling and Simulation, Master's Thesis - European Astronaut Centre (ESA) / ISAE-SUPAERO, 2017.

[12] R.H. Turner, Space power system utilizing Fresnel lenses for solar power and also thermal energy storage, in: Eighteenth Intersoc. Energy Convers. Eng. Conf., American Institute of Chemical Engineers, Orlando (FL), 1983: pp. 971–976.

[13] A.V. Lozano, Development of a Lunar Regolith Thermal Energy Storage Model for a Lunar Outpost, Master's Thesis - European Astronaut Centre (ESA) / Université Paul Sabatier Toulouse III, 2016.

[14] A. Colozza, Analysis of Lunar Regolith Thermal Energy Storage, 1991.

[15] H.L. Jones, J.P. Thornton, R. Balasubramaniam, S.A. Gokoglu, K.R. Sacksteder, W.L. Whittaker, Enabling Long-Duration Lunar Equatorial Operations With Thermal Wadi Infrastructure, 2011. https://ntrs.nasa.gov/archive/nasa/casi.ntrs.nasa.gov/20110007929.pdf.

[16] P.L. Córdoba, Thermal Energy Storage Demonstrator, Master's Thesis - European Astronaut Centre (ESA) / UPC, 2017.

[17] A.R. Vasavada, J.L. Bandfield, B.T. Greenhagen, P.O. Hayne, M.A. Siegler, J. Williams, D.A. Paige, Lunar equatorial surface temperatures and regolith properties from the Diviner Lunar Radiometer Experiment, J. Geophys. Res. 117 (2012) 1–12.

644 doi:10.1029/2011JE003987.

645 [18] M.T. Mellon, B.M. Jakosky, H.H. Kieffer, P.R. Christensen, High-Resolution Thermal
646 Inertia Mapping from the Mars Global Surveyor Thermal Emission Spectrometer, Icarus.
647 148 (2000) 437–455. doi:10.1006/icar.2000.6503.

648 [19] G. Heiken, D. Vaniman, B.M. French, Lunar sourcenook: A user's guide to the Moon,
649 (1991).

650 [20] A.R. Vasavada, D.A. Paige, S.E. Wood, Near-Surface Temperatures on Mercury and the
651 Moon and the Stability of Polar Ice Deposits, Icarus. 141 (1999) 179–193.

652 [21] B.S. Hemingway, R.A. Robie, W.H. Wilson, Specific heats of lunar soils, basalt, and
653 breccias from the Apollo 14, 15, and 16 landing sites, between 90 and 350°K, in: Lunar
654 Sci. Conf. 4th, SAO/NASA Astrophysics Data System (ADS), n.d.: pp. 2481–2487.

655 [22] M.G. Langseth, S.J. Keihm, K. Peters, Revised lunar heat-flow values, in: Lunar Sci.
656 Conf. 7th, Houston, Texas, SAO/NASA Astrophysics Data System (ADS), 1976: pp.
657 3143–3171.
658 http://articles.adsabs.harvard.edu//full/1976LPSC....7.3143L/0003169.000.html.

659 [23] D.L. Mitchell, I. De Pater, Microwave Imaging of Mercury's Thermal Emission at
660 Wavelengths from 0.3 to 20.5 cm, Icarus. (1994) 2–32.

661 [24] C.J. Cremers, Thermophysical Properties of Apollo 12 Fines, Icarus. 18 (1973) 294–303.

662 [25] R. Morrel, Thermal conductivities, Tables Phys. Chem. Constants. (n.d.).
663 http://www.kayelaby.npl.co.uk/general_physics/2_3/2_3_7.html (accessed February 3,
664 2018).

665 [26] W. Callister, D. Rethwisch, Materials science and engineering: an introduction, in: Mater.
666 Sci. Eng., 2007: pp. 266–267. doi:10.1016/0025-5416(87)90343-0.

667 [27] H. Alam, S. Ramakrishna, A review on the enhancement of figure of merit from bulk to
668 nano-thermoelectric materials, Nano Energy. 2 (2012) 190–212.

669 doi:10.1016/j.nanoen.2012.10.005.

670 [28] H. Tsai, J. Lin, Model Building and Simulation of Thermoelectric Module Using Matlab /
671 Simulink, J. Electron. Mater. 39 (2009) 2105–2111. doi:10.1007/s11664-009-0994-x.

672 [29] Termo-Gen AB, Datasheet Bismuth telluride TEG Modules (TEP1- 12656-0.6), (2006).
673 http://www.termo-gen.com/pdf/TEG_modules_Bi2Te3.pdf (accessed April 15, 2019).

674 [30] E. Kanimba, Z. Tian, Modeling of a Thermoelectric Generator Device, in: InTechOpen,
675 2016: pp. 461–479.

676 [31] D. Tatarinov, M. Koppers, G. Bastian, D. Schramm, Modeling of a Thermoelectric
677 Generator for Thermal Energy Regeneration in Automobiles, J. Electron. Mater. 42
678 (2013) 2274–2281. doi:10.1007/s11664-013-2642-8.

679 [32] TEC Solidstate Power Generators, Datasheet for High Efficiency Pb/TAGS TEG
680 Modules (PBTAGS-200:009A10), (n.d.). http://tecteg.com/wp-
681 content/uploads/2016/05/PBTAGS-200.009A10.pdf (accessed April 15, 2019).

682 [33] K. Romanjek, S. Vesin, L. Aixala, T. Baffie, J. Dufourcq, High-Performance Silicon –
683 Germanium-Based Thermoelectric Modules for Gas Exhaust Energy Scavenging, J.
684 Electron. Mater. 44 (2015) 2192–2202. doi:10.1007/s11664-015-3761-1.

685 [34] C. Nicollier, Particle Flux in the Earth Environment, 2019.

686 [35] R. Balasubramaniam, R. Wegeng, S. Gokoglu, N. Suzuki, K. Sacksteder, Extended-
687 Duration Lunar Exploration, 2010.
688 https://ntrs.nasa.gov/archive/nasa/casi.ntrs.nasa.gov/20100015637.pdf.

689

Appendix A – Thermoelectric Materials Properties

Table A.1: Thermoelectric generator properties for the three selected materials Bi2Te3: [29], PbTe/TAGS [32], and SiGe [33]. The data obtained from the datasheet for Bi_2Te_3 and PbTe/TAGS are constant but from commercially available TEGs. Data on SiGe taken from [33]. The resulting equations given for SiGe were obtained through polynomial fitting trend lines for these sources.

Properties of TC	**Value / function of temperature**
Bi_2Te_3 [29]	
Temperature range (K)	200 to 500
Internal resistance of a TC $(\mathrm{m\Omega})$	9.75
Seebeck coefficient $(\mu \mathrm{V.K^{-1}})$	372.2
Figure of Merit $(-)$	0.86
PbTe/TAGS [32]	
Temperature range (K)	300 to 700
Internal resistance of a TC $(\mathrm{m\Omega})$	11.4
Seebeck coefficient $(\mu \mathrm{V.K^{-1}})$	280
Figure of Merit $(-)$	0.85
SiGe [33]	
Temperature range (K)	500 to 1000
n-type resistivity $(\Omega.\mathrm{m})$	$-4.73 \times 10^{-14} \cdot T^3 + 7.86 \times 10^{-11} \cdot T^2 - 1.96 \times 10^{-8} \cdot T + 2.54 \times 10^{-}$
p-type resistivity $(\Omega.\mathrm{m})$	$6.51 \times 10^{-12} \cdot T^2 + 9.75 \times 10^{-9} \cdot T + 7.4 \times 10^{-6}$
Seebeck coefficient $(\mathrm{V.K^{-1}})$	$-2 \times 10^{-10} \cdot T^2 + 6.39 \times 10^{-7} \cdot T + 1.06 \times 10^{-4}$
Figure of Merit $(-)$	$ZT_{n-type}Z_{T_{n-type}}(T_{hot}) = 4.286 \times 10^{-7} \cdot {T_{hot}}^2 + 7.589 \times 10^{-4} \cdot T_{hot} - 0.1720$

Appendix B – Trade-off analysis

The details of the trade-off analysis performed to compare four systems to satisfy the power demand during the polar night at the specified location are presented here. Table B.1 shows the cooperative method that has been used to assign the weights to each criterion. Table B.2 shows the scoring rules for each criterion. Table B.3 shows the systematic approach to determine the figure of merit of each approach with respect to the proposed criteria.

Table B.1 Trade-off weights were averaged after independent consultation of 4 researchers within the team (anonymously identified by A, B, C and D). The highest is the weight, the most it will affect the total scores.

Criterion/Researcher preferred weights	**A**	**B**	**C**	**D**	**Average Weight**
Mass of the Power System	5	5	3	4.5	**4.4**
Global Specific Power	1.5	1	4	1.5	**2.0**
Space Heritage	2	2	4	3.5	**2.9**
System Complexity	2.5	4	4	1	**2.9**
Installation Efforts	2.5	3	5	2.5	**3.3**
Operations	3	3	3	1.5	**2.6**
Scalability	2	1	3	4	**2.5**
Lifespan	3	4	5	4.75	**4.2**
Potential benefit for Earth	0.5	1	1	0.25	**0.7**
End-of-life	1	2	1	0.25	**1.1**

710 **Table B.2** Trade-off scoring rules. Each system scores +5; +3; +0 or -3 points per criterion

711 depending on the scoring rules. The total score is calculated with a weighted average.

Criteria / Scoring (points)		**Good (+5)**	**Medium (+3)**	**Bad (0)**	**Very Bad (-3)**
Power System Mass	[kg]	< 10000	10000 - 20000	20000 - 30000	> 30000
Global Specific Power	[$W.kg^{-1}$]	> 2	2-1	1-0.25	< 0.25
Space Heritage	TRL	6 or +	4-5	2-3	1
System Complexity	[see index]	1 or less	2-3	4-5	> 5
Installation Efforts	[see index]	0	1-2	3-4	5
Operations	[see index]	1 or less	2-3	4	> 4
Scalability	[-]	5W - 100kW	High-power only	low-power only	no
Lifespan	[years]	> 15	10-15	4-10	< 4y
Potential benefit for Earth	[-]	Strong	Possible	Unlikely	No
End-of-life	[see index]	3	2	1	0

712

713

714 **Table B.3** Criteria assessment and justifications

Power System Mass

All masses were estimated using the internal ESA mass budget tool. The given figures include a safety factor of 1.5 to applied on the energy storage requirement.

1. Solar Arrays & Batteries: **17867 kg (bad)**
    i. 222 kg of solar arrays
    ii. 14667 kg of batteries (Li-ion)
    iii. 2978 kg for harness, structure, and power control and distribution unit
2. Solar Arrays & Regenerative Fuel Cells: **6507 kg (Medium)**
    i. 1256 kg of solar arrays
    ii. 211 kg of electrolyzers
    iii. 40 kg of fuel cells
    iv. 4750 kg of hydrogen and oxygen tank dry mass
    v. 250 kg of power control and distribution unit.
    vi. (optional 1600 kg of water that could be brought from Earth or mined on the moon)
3. Fission Surface Power: **3700 kg (Good)**
    No storage required
4. Thermal Energy Storage: **83205 kg (Very Bad)**
    i. 420 TES/TEG units required
    ii. 2 Hot sink plate per unit: 3.24 kg
    iii. Thermal beam per unit: 8.1 kg
    iv. 5m^2 radiator per unit: 33.75 kg
    v. 21m^2 Fresnel lens per unit: 84 kg
    vi. 30 m^2 reflectors per unit: 30 kg
    vii. Heat Pipes per unit: 6 kg
    viii. Holding Structure, sun-trackers, Power control distribution unit (optimistic 20%): 33 kg
    ix. Total is 198 kg per unit

Global Specific Power

1. Solar Arrays & Batteries: **0.56 W/kg (Bad)**
2. Solar Arrays & Regenerative Fuel Cells: **1.54 W/kg (Medium)**
3. Fission Surface Power: **2.7 W/kg (Good)**
4. Thermal Energy Storage: **0.12 W/kg (Very Bad)**

Space Heritage

1. Solar Arrays & Batteries: **TRL 9 (Good)**
2. Solar Arrays & Regenerative Fuel Cells: **TRL 6+ (Good)**
3. Fission Surface Power: **TRL 4 (Medium)**
4. Thermal Energy Storage: **TRL 2-3 (Bad)**

System Complexity (high index is bad)

The scoring rules refers to a system complexity index computed by addition of the points recommended if applicability of the following statement:

- Slow-motion or occasionally moving parts? (+1)
- High-velocity moving parts? (+3)
- Non-hazardous, easy to store working fluid? (+1)
- One hazardous, difficult to store working fluid? (+2)
- Multiple working fluids? (+3)
- Considerable vibrations? (+1)
- Tendency to be unstable, uncontrollable (+1)

1. Solar Arrays & Batteries: **complexity index = 1 (Good)**
2. Solar Arrays & Regenerative Fuel Cells: **complexity index = 4 (Bad)**
3. Fission Surface Power: **complexity index = 8 (Very Bad)**
4. Thermal Energy Storage: **complexity index = 2 (Medium)**

Installation Efforts on the Moon (high index is bad)

The scoring rules refers to a installation index computed by addition of the points recommended if applicability of the following statement:

- A couple of hours of work, almost plug and play and can be done robotically (+0)

- Humans required on-site for installation, only a few hours of work (+1)
- Little ISRU, be can be avoided with extra-mass brought from Earth (+2)
- Significant ISRU required (+3)
- More than 300 manned hours of installation (+3)

1. Solar Arrays & Batteries: **installation index = 0 (Good)**
2. Solar Arrays & Regenerative Fuel Cells: **installation index = 2 (medium)**
3. Fission Surface Power: **installation index = 2 (medium)**

   (A Fission Surface Power plant shall be installed autonomously before the arrival of the crew to minimize risks. It could be assisted by robots, or self-deployable. The fission reaction can be started only when the reactor is on-site. There are not significant installation efforts to be made, because it shall be made autonomously or robotically.)
4. Thermal Energy Storage: **complexity index = 5 (Very Bad)**

   (In order to install such system with 420 units to satisfy the 10kW power, we estimate the mass to be sintered to be 246 metric tons. This is considerable and would require specialized rover, and already utilize tremendous amount of energy in the building phase.)

Operations (high index is bad)

The scoring rules refers to an operations index computed by addition of the points recommended if applicability of the following statement:

- Any serious safety issue, for transportation, launch or work around the base? (+2)
- Weekly maintenance estimated > 2hrs? (+1)
- Needs of Astronauts daily intervention > 30min (+2)
- Critical, non-repairable element? (+2)
- Remote monitoring necessary from Earth? (+1)

1. Solar Arrays & Batteries: **operations index = 0 (Good)**
2. Solar Arrays & Regenerative Fuel Cells: **operations index = 1 (Good)**

   (high-pressure systems to be monitored)
3. Fission Surface Power: **operations index = 4 (Bad)**

There is of course safety issue with nuclear power sources, and most of the parts in the core of the system will be neither replaceable nor repairable by astronauts, but this task will be done robotically. Due to its nature, operations performed by astronauts will be minimized if no banned. Mostly, the reactor will be monitored remotely.

4. Thermal Energy Storage: **complexity index = 1 (Good)**

Scalability

1. Solar Arrays & Batteries: **5W – 100kW (Good)**
2. Solar Arrays & Regenerative Fuel Cells: **high-power mostly (Medium)**
3. Fission Surface Power: **high power only (Medium)**
4. Thermal Energy Storage: **low power only (Bad)**

Lifespan

1. Solar Arrays & Batteries: **10 – 15 years (Medium)**

   Lifespan limited by the battery lifetime which represent most of the subsystem mass.
2. Solar Arrays & Regenerative Fuel Cells: **10 years (Medium)**
3. Fission Surface Power: 5 to 10 **(Bad)**
4. Thermal Energy Storage: **> 15 years (Good)**

Potential benefits for Earth systems

1. Solar Arrays & Batteries: **possible (Medium)**
2. Solar Arrays & Regenerative Fuel Cells: **strong (Good)**

   (hydrogen very much regarded as future energy vector)
3. Fission Surface Power: **unlikely (Bad)**
4. Thermal Energy Storage: **possible (Medium)**

End-of-life (high index => good)

The scoring rules refers to an End-of-Life index computed by addition of the points recommended if applicability of the following statement:

- Significant recyclability? (+3)
- Little recyclability? (+2)
- Not recyclable but no EOL constraints? (+1)

- Significant EOL constraints (0)

1. Solar Arrays & Batteries: **1 (Bad)**
2. Solar Arrays & Regenerative Fuel Cells: **1(Bad)**
3. Fission Surface Power: **0 (Very Bad)**
4. Thermal Energy Storage: **2 (Medium)**

715

Highlights:

ISRU approaches are not systematically preferable to Earth supplied infrastructures.
Thermoelectricity generation from lunar thermal energy storage is not attractive.
A 200-kg TES/TEG system using lunar regolith could produce 36 W during a polar night.

In-Situ Approach for Thermal Energy Storage and Thermoelectricity generation on the Moon: Modelling and Simulation

Authors:

Patrick Fleith[ab*], Aidan Cowley[a], Alberto Canals Pou[ac], Aaron Valle Lozano[ade], Rebecca Frank[a], Pablo Lopez Cordoba[af], Ricard González-Cinca[f]

[a] *European Astronaut Centre (ESA/EAC), Linder Hoehe D-51147, Cologne, Germany*

[b] *ISAE-SUPAERO, 10 Avenue Edouard Belin, 31400 Toulouse, France*

[c] *Department of Materials Science and Metallurgy (CMEM), ETSEIB, Universitat Politècnica de Catalunya (UPC), Avda. Diagonal 647, 08028 Barcelona, Spain*

[d] *Luleå University of Technology, RYMDCAMPUS 1, 98192 Kiruna, Sweden*

[e] *Université Toulouse III - Paul Sabatier, Route de Narbonne, 31330 Toulouse, France*

[f] *Technical University of Catalonia-Barcelona Tech (UPC) c/ E. Terradas, 5. 08860 Castelldefels, Barcelona, Spain*

** Corresponding Author*

Abstract

Human, tele-operated rovers, and surface infrastructures are now being actively considered for lunar polar exploration. Current approaches to energy provision consider, among others, hybrid direct energy/chemical technologies, such as solar photovoltaic arrays, batteries, and regenerative fuel cells. Due to the long period of darkness on the Moon and the challenges this poses to the aforementioned conventional energy generation and storage technologies, there is a need to assess the potential of In-Situ Resources Utilization (ISRU) methods to enable or supplement long duration missions. We present a computational model (MATLAB) of a Thermal Energy Storage (TES) system coupled to drive a heat engine (Thermoelectric Generator) to produce electricity. The TES medium designed is based off processed lunar regolith, an abundant material present on the surface of the Moon. The architecture has been optimized to provide a minimum electrical power of 36 W per unit after 66 hours of polar night, but the modular nature of the model allows other ranges of parameter to be simulated. A trade-off between this ISRU-based concept and conventional approaches for energy production and storage was performed and ranked TES and thermoelectricity generation as the least appropriate option. This result is valuable in a period of enthusiasm towards ISRU. It shows that processes exploiting extraterrestrial materials instead of Earth supplies are not systematically attractive. Despite the non-favorable performances for the proposed concept, some perspectives for the TES system are given as well as potential model improvements such as the need to assess the use of a Stirling heat engine.

Keywords: Thermal Energy Storage; Thermoelectric; MATLAB; Moon; ISRU

Abbreviations:

- ESA: European Space Agency
- EVA: Extra-Vehicular Activity
- ISRU: In-Situ Resources Utilization
- ISS: International Space Station
- PDE: Partial Differential Equation
- SEC: Solar Energy Collector

- TC: Thermocouple
- TE: Thermoelectric
- TEG: Thermoelectric Generator
- TES: Thermal Energy Storage
- TM: Thermal Mass

1. Introduction

There is a renewed interest in returning astronauts to the Moon and establishing a sustainable human exploration capability on its surface. Indeed, the “Moon Village” concept was initiated by Jan Woerner, Director General of the European Space Agency (ESA), and is part of the vision of Space 4.0, a set of concrete actions for returning to the Moon in an environment for international cooperation and commercialization of space [1].

One of the greatest challenges in the exploration of the Moon, which is addressed from an ISRU perspective in this paper, is the storage of energy for missions involving lunar nighttime. Pragmatically, the rim of the Shackleton crater at the South Pole of the Moon is not only a key target of interest for science and exploration but it also allows substantial sun visibility [2], which reduces the potential complexity and mass of a stand-alone power system. Due to the prohibitive cost of transportation of materials from Earth, there is a need to assess In-Situ Resources Utilization (ISRU) approaches for energy production and storage. As ISRU has been identified as a key element to facilitate sustainable presence of humans in outer space (on the Moon or Mars), numerical modelling and simulation can enable us to assess its potential, and to compare it with other approaches. It is expected that through a smart use of ISRU, most of the systems could be built out of locally available resources, which would drastically decrease the amount of equipment launched from Earth. Nevertheless, the use of ISRU technologies has sometimes been questioned [3]. In this paper we propose and model a system for thermal energy storage in processed lunar regolith and electricity generation by means of thermoelectric converters. The advantages and disadvantages of the system with respect to other approaches have been analyzed in order to determine if the proposed concept has merit. The paper is organized as follows:

- Section 2 describes a realistic exploration scenario in the South Pole of the Moon, and its challenges in terms of energy production and storage. The variable sunlight conditions are addressed, and a plausible illumination profile is derived.
- An ISRU-based concept for Thermal Energy Storage on the Moon associated with Thermoelectric Generators (TES/TEG) is introduced in Section 3.

- Section 4 describes an integrated MATLAB model of the TES/TEG concept. The description includes the assumptions, data, and equations that have been used to build the model, such as temperature-dependent properties of regolith and thermoelectric materials.
- A trade-off analysis is presented in Section 5, in which the TES/TEG concept is compared to power subsystems based off solar arrays and batteries, solar arrays and regenerative fuel cells, and fission surface power. The trade-off analysis has ranked the TES/TEG concept as the least favorable alternative. It suggests that the concept and technologies need significant improvements to become more practically attractive. Therefore, a list of recommendations to improve the model and some general perspectives regarding ISRU-based thermal energy storage are provided in Section 6.

2. Exploration scenario of the Moon and the challenge of energy production and storage

2.1 Reasons for exploration of lunar South Pole

One of the major challenges for a long duration human surface mission will be provision of energy due to protracted darkness during the nighttime. The synodic period of the Moon is 29.54 days (709 hrs) [4]. At equatorial regions of the Moon, the lunar night can last up to 350 hours which is much longer than in the ISS (eclipses of 45 min). Therefore, the energy to be stored in order to meet a similar power demand would significantly increase on the Moon. In case batteries were used for energy storage, its number would be at least two orders of magnitude larger than in the ISS, which would lead to a dramatic increase of mass to be launched from Earth. Lunar poles are regions that benefit from long periods of sunlight due to the low elevation angle of the Sun and local topography [2]. Therefore, photovoltaic panels could be used for long periods, which would reduce the energy to be stored for the dark periods.

The polar temperature variations can be smaller at lunar poles (50°C) than at the equator (250°C) [5] which is an advantage for materials and infrastructures which are sensitive to degradation from high-amplitude thermal cycling [4]. However, the local topography and sun elevation at the poles could cause the number of thermal cycles to be greater than elsewhere on the Moon which affects planetary systems design.

Several lunar observation missions delivered evidence of the presence of water in the form of ice located in permanently shadowed regions near poles. Volatile water can be trapped in cold places such as these regions. The LCROSS mission estimated a mass concentration of water ice in the regolith of $5.6 \pm 2.9\%$ [6]. Water is of high importance to support human presence since drinkable water can be obtained from it, and O_2 and H_2 can be obtained by means of electrolysis.

The primary interest for lunar surface missions is the access to relevant terrains for science and exploration preparation, whereby geological, geophysical and geochemistry research can be performed and exploration enabling technologies can be demonstrated in-situ. In addition, the

aforementioned reasons for exploration of lunar South Pole are strong enablers for mission feasibility.

2.2 Determination of the illumination profile at the rim of the Shackleton crater

In order to study the potential of a solar-based concept for energy production and storage, it is necessary to identify the illumination profile at the target location. The South Pole presents some sites with high levels of sun visibility. These areas are located near the Shackleton crater, as depicted by the illumination map in Figure 1. They present high solar visibility, and a maximum continuous polar night significantly shorter than at equatorial regions.

In the considered scenario, any asset placed on the Moon's surface would experience a period of darkness between 100 and 250 hours maximum. However, two meters above the surface, the illumination conditions are much better. At a position of latitude -89.6866°N and longitude 197.19°E, the solar visibility is estimated to be 89.4% (over a 20-year period) and the maximum time continuously in shadow is 66 hours [2]. This illumination condition represents therefore the best-case scenario (in term of longest darkness period) to study the feasibility of the concept. We assume that the solar energy collector would be mounted 2 m above the surface in order to increase solar visibility. This is possible since quantitative values are available from the literature as an input to our analysis [2]. One might argue that, instead, the worst illumination case scenario should be assessed. However, since the objective of this work is to determine if the proposed concept has merit, any negative assessment in the best-case scenario would also eliminate the choice of this power supply alternative for harsher conditions.

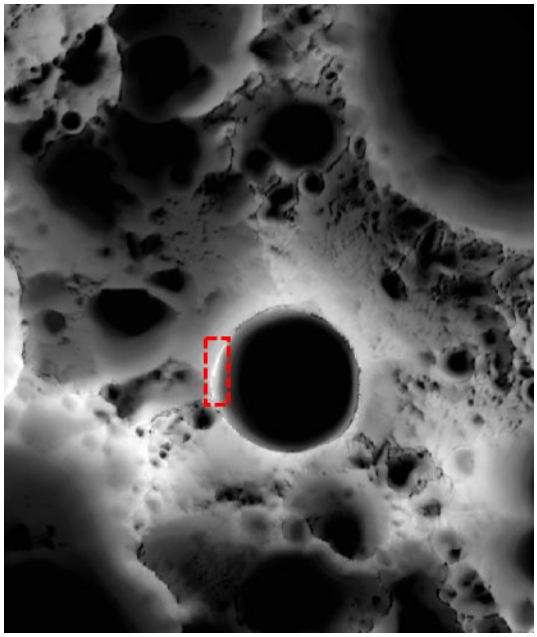

Figure 1: Multi-temporal illumination map of the lunar South Pole. The Shackleton crater (19 km diameter) is in the center. The South Pole is located approximately at 9 o'clock on its rim (highlighted region). Mapped area extends from 88°S to 90°S [7].

3. Thermal energy storage concept for electricity generation

An ISRU approach as a means of energy provision is to use the lunar regolith as the medium for thermal energy storage [8,9], similar to the underground thermal energy storage concept used on Earth. Heat can be stored in solid materials (thermal mass) in the form of sensible heat. A hot heat transfer fluid passes through the thermal mass heating it. If the heat losses are minimized, the thermal mass can be kept at high temperature, until the energy is released using the reverse mechanism. In this case, a cold working fluid passes through the thermal mass and absorbs the heat. The temperature of the fluid increases, which can be used as the source for a heating system.

The thermal masses can be fabricated at the Moon using sintered regolith. Sintering is accomplished by compacting loose material (powders, lunar dust) and forming a solid mass of material by applying heat and/or pressure. During this process, particles form strong bonds with a reduction in the volume of pores, with an attendant change in other material characteristics (e.g. bulk thermal conductivity). It has been demonstrated on Earth that lunar regolith simulant

can be processed into solid blocks (lunar bricks) with higher thermal conductivity than native regolith (by a factor 200). A 1.5 tons block made of lunar regolith simulant was 3D printed for proof of principle demonstration at the European Space Agency [10].

Figure 2 shows the proposed energy storage concept coupled with a heat engine. The concept is based on the thermal energy storage systems proposed in [8,9]. The system contains the following components: a solar energy concentrator to focus the incident sunlight and achieve a high heat flux; a thermal mass made of sintered regolith which is heated by the concentrated flux; a heat engine that converts the thermal energy into electricity, and a radiator that keeps the cold sink at low temperature. The different subsystems are described in the following modelling section.

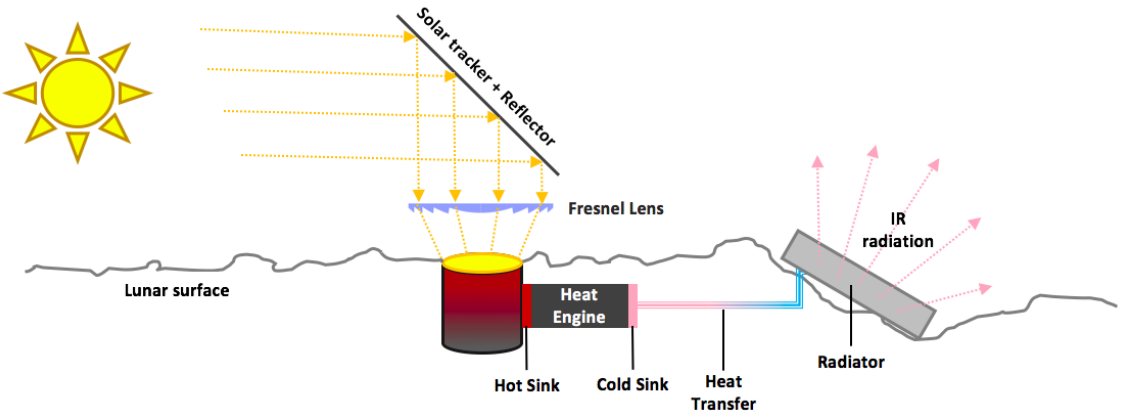

Figure 2: Thermal Energy Storage system coupled with a heat engine for electricity generation, and a radiator to cool down the cold sink.

4. Modelling the TES/TEG system

This section details the assumptions, data, and equations used to build the model for further assessment of the potential of the TES/TEG concept. The model has been implemented in MATLAB R2017b [11].

4.1 Modelling the solar energy collector

The objective of the Solar Energy Collector (SEC) is to collect and concentrate the solar flux to reach the high temperature desired for the thermal mass to store energy. The SEC is composed of a reflector and a concentrator. The reflector consists of a reflective mirror surface that can track the Sun position. The reflector is able to re-direct a high incidence flux perpendicularly to the target surface. Since a normal incidence flux is not sufficient, a Fresnel lens can be used to concentrate the Sun flux [12].

We assume that a reflector can ensure a minimum flux of $1000\ \mathrm{W.m^{-2}}$ during the polar day. This is acceptable given the general incoming solar flux on the Moon (neglecting ephemeris variations) is $\phi_{\mathrm{sun}} = 1365\ \mathrm{W.m^{-2}}$. The assumed lower value of the flux provided by the reflector accounts for efficiency of the mirrors (secular reflectivity estimated to be 85 to 90%), misalignments, actuation and geometrical limits. Thus, the heat flux given by the reflector is:

$$\phi_R = \begin{cases} 1000\ \mathrm{W.m^{-2}} & \text{(in sunlight)} \\ 0\ \mathrm{W.m^{-2}} & \text{(in shadow)} \end{cases} \qquad (1)$$

The concentrated flux of the SEC is given by:

$$\phi_C = f \cdot \eta_{FL} \cdot \phi_R\ , \qquad (2)$$

where f is the magnification of the Fresnel lens and η_{FL} its efficiency. With $f = 70$, a reflected flux of $1\ \mathrm{kW.m^{-2}}$ can be concentrated to achieve almost $70\ \mathrm{kW.m^{-2}}$. It is assumed that a magnification of $f = 70$ and only 5% of transmission losses can be achieved for a Fresnel lens optimized for the Moon. These assumptions are the basis for the concentrated solar flux and enable the top surface temperature of the thermal mass to reach about 1000 K [13].

4.2 Modelling the thermal mass

The Thermal Mass (TM) thermally stores the energy and serves as a hot source for the heat engine. It is made of sintered regolith and buried into the lunar native regolith to mitigate heat losses. Indeed, the native regolith acts as insulator material, owing to its low thermal conductivity. No loop heat pipes were considered inside the TM since its conductivity is already enhanced with the sintering process. (average values of 2.1 $W.K^{-1}.m^{-1}$) for sintered regolith against 0.01 $W.K^{-1}.m^{-1}$) for native regolith [14,15])

The model of the TM was implemented with the Partial Differential Equations (PDE) toolbox of MATLAB. A 2D-model is chosen because a vertical cross-section of the entire TM is sufficient to study the system. In previous studies, a cylindrical geometry of 0.5 m in height and 0.3 m in diameter was considered [13,16]. These values are closely linked to manufacturing capability of sintering methods. Because in this concept the TM is buried into lunar soil, automotive rovers or astronauts would have to drill and excavate native regolith. The level of difficulty to perform this operation for depths greater than 0.5 m – 1m is not well known. Sintering lunar rovers would also have limited size. Therefore, the diameter is set to 0.3 m. These values were initially used for the model and ultimately set to a depth of 0.65 m and width of 0.3 m for optimized performances.

Figure 3 shows the designed TM buried into native regolith. At the top of the native regolith, a 'fluff' layer of regolith is modelled (with a very low thermal conductivity, see Table 1 and Equation 7). On each side of the TM, an interface (hot sink plate) is modelled, and a hole is defined within this geometry to model the presence of a TEG module. The overall model does not have a meshed TEG since all computations for thermal transfers are done with a TEG MATLAB function. We assume that the cold side of the TEG is connected to a cold plate which rejects the heat through the radiator. Heat transfer from the TEG cold side to the radiator are not implemented in this geometry since it is implemented in a separate function. Additionally, a thermal conductance beam is modelled vertically in the middle of the TM in order to enhance heat propagation through the medium. Although sintered regolith has a larger thermal conductivity than fluff regolith, and thus a larger heat transfer rate, the optimization process of

this work showed that the presence of a thermal beam substantially increases the system performance.

The PDE toolbox automatically generates the mesh and increases the number of nodes where it is needed (see Figure 3).

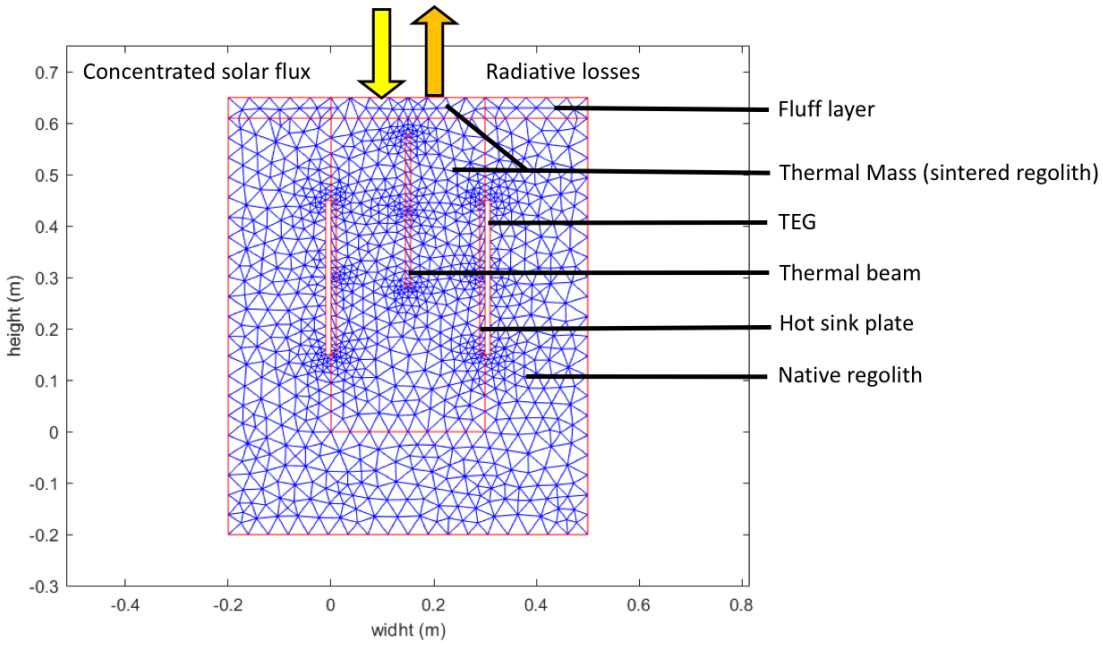

Figure 3: 2D-Model of the TM buried into lunar native regolith with a thermal beam in the middle and TEG modules on each side (white rectangles) attached to the hot sink plates. Note that the fluff layer does not extend on the top of the TM. The rectangle at the top of the TM is actually part of the sintered regolith block as pointed out on the figure.

The thermal mass model element can return the temperature at any time during the simulation as we solve a transient heat transfer problem with temperature dependent properties. The model accounts for heat gain from the Sun, losses, and energy extracted for power generation. The associated partial differential equation to be solved for conductive heat transfer is:

$$\rho \cdot c_p(T) \cdot \frac{\partial T}{\partial t} - \nabla \cdot (\kappa(T) \cdot \nabla T) = h, \quad (3)$$

where ρ is the density of the body, $c_p(T)$ its specific heat, T is the body's temperature, $\kappa(T)$ its thermal conductivity, and h is the heat generated inside the body. In order to solve Eq. 3, the properties of sintered regolith, native regolith, and fluff layer are provided as inputs (Table 1).

The surface emissivity of sintered regolith is assumed to be similar to native regolith emissivity. The surface absorptivity is assumed to be 0.85 since the Moon albedo ranges from 0.1 to 0.2 and the mean value for the surface of the Moon is 0.15 [17]. During the polar night, the surface emissivity of the TM is reduced by a factor 50 in order to account for radiative losses mitigation. This can be practically done by employing a highly reflective/insulating cover cap which covers the top of the TM during the polar night. This could be made with Multi-Layer Insulation (MLI) which has a high insulating performance (0.0006 $W.K^{-1}.m^{-1}$ for a 40-layer MLI) [3].

Table 1: Properties of native and fluff regolith. Sintered regolith properties are taken similar to basalt rock.

Properties	Native Regolith	Fluff layer	Sintered Regolith (basalt rock)
Density $(\mathrm{kg.m^{-3}})$	1800 [8]	1300 [18,19]	3000 [8]
Specific heat $(\mathrm{J.kg^{1}.K^{-1}})$	840-850 [8,14]	840-850 [8,14]	800 [8]
Thermal conductivity $(\mathrm{W.K^{-1}.m^{-1}})$	9.3×10^{-3} [8,14]	2.29×10^{-3} [18]	2.1 [8]
Surface emissivity $(-)$	0.96 [20]	0.96 [20]	0.96 [20]
Surface absorptivity $(-)$	0.85 [17]	0.85 [17]	0.85 [17]

It is important to implement the temperature dependence of the TM properties due to the large temperature variations. An expression for TM conductivity was obtained from a curve fit and interpolation of experimental data provided in the literature for the specific case of sintered lunar rock (resolidified) [14,21]:

$$\kappa_{TM}(T) = 6 \times 10^{-7} \cdot T^2 - 0.0028 \cdot T + 3.3753 \qquad (4)$$

Similarly the specific heat for lunar sintered regolith has been fitted to the following expression [14,22]:

$$c_{pTM}(T) = -5 \times 10^{-4} \cdot T^2 + 1.4332 \cdot T + 371.5 \qquad (5)$$

The native regolith conductivity [20,23]:

$$\kappa_{nat}(T) = 0.0093 \cdot \left\{1 + 0.073 \cdot \left(\frac{T}{350}\right)^3\right\} \qquad (6)$$

The fluff regolith layer conductivity [20,24]:

$$\kappa_{fluff}(T) = 9.22 \times 10^{-4} \cdot \left\{1 + 1.48 \cdot \left(\frac{T}{350}\right)^3\right\} \qquad (7)$$

Eqs. 3 to 7 and Table 1 are used to compute the conductive heat transfer between the thermal mass and the surrounding regolith. Convection mechanism are not considered since there is nearly vacuum on the Moon. The remaining losses are radiative heat losses, which are given by:

$$\phi_{rad} = \varepsilon_{TM} \cdot \sigma \cdot \left(T_{top}^4 - T_{space}^4\right), \qquad (8)$$

where ϕ_{rad} is the radiative flux, ε_{TM} is the emissivity of the TM, σ is the Stefan-Boltzmann constant (5.67×10^{-8} W.m^{-2}K^{-4}), T_{top} is the temperature of the top surface of the TM facing outer space, T_{space} the temperature of deep space usually taken at 3 K. During the polar night $\varepsilon_{TM}(night)$ is taken as $\varepsilon_{TM}(day)/50$.

In order to compute the temperature in the TM, an initial temperature of the system has to be selected. 254 K is the bulk temperature beyond the thermal penetration depth of the lunar soil. The penetration depth usually ranges from 0.2 to 0.3 m. Therefore, the bottom boundary of the TM is set at a constant temperature of 254 K. To fix a constant temperature on a boundary, a *Dirichlet* boundary condition is employed in MATLAB.

The TM model also takes into account heat gain from the Sun flux and heat losses towards deep space (conduction losses are directly simulated by the model since native regolith surrounds the TM geometry). The TM receives a constant flux from the SEC during the polar day given by:

$$\phi_{SEC \to TM} = \alpha_{TM} \cdot \phi_C \qquad (9)$$

$\alpha_{TM} = 0.85$ being the absorptivity of the TM.

The net flux absorbed by the element is given by $\phi_{SEC \to TM}$ and the radiation losses:

$$\phi_{net}(T) = \phi_{SEC \to TM} - \phi_{rad}(T) \qquad (10)$$

$\phi_{net}(T)$ is set as a *Neumann* boundary condition in MATLAB at the top surface of the TM.

The general form of the partial differential equation solved by the MATLAB PDE Toolbox is:

$$m\frac{\partial^2 u}{\partial^2 t} + d\frac{\partial u}{\partial t} - \nabla \cdot (c\nabla u) + au = z, \quad (11)$$

Where in our model u corresponds to temperature and the coefficients are given by: $m = 0$, $d = \rho \cdot cp(T)$, $c = \kappa(T)$, and $z = h = 0$ (no heat generated in the system).

Unlike PDE's coefficients, *Neumann* boundary conditions cannot be set as temperature-dependent in the PDE toolbox of MATLAB. In order to overcome this problem, the simulation computes the temperature profile with a value of ϕ_{net} that is updated with the new temperature values at the end of each time step in the code. The time step was kept below 100 sec due to convergence issues if exceeding 120 sec.

4.3 Modelling the thermoelectric generator

The Thermoelectric Generator (TEG) consists of an array of thermocouple materials assembled in series, sandwiched into two plates: one hot and one cold sink plates. The plates serve as interfaces between the thermoelectric array: on one side with the hot thermal mass, and on the cold side with the radiator where the wasted energy is dissipated (see Figure 2 and Figure 3). These plates are assumed to be a thin interface made of conductive material in order to provide a homogeneous temperature for all thermocouples attached to it. Aluminum prevails in lunar regolith, mostly in form of oxides. Therefore, due to its high thermal conductivity and availability on-site, Aluminum was chosen as a good test candidate for the plates (see properties of Aluminum in Table 2). A conservative value for the thermal conductivity is taken to account for impurities and performance degradation due to thermal cycling.

Table 2: Properties of Aluminum used to model the hot and cold sink plates [25,26].

Properties	Hot/cold Sink Plate
Density (Al) $(\mathrm{kg.m^{-3}})$	2700
Specific heat (Al) $(\mathrm{J.kg^{-1}.K^{-1}})$	900

Thermal conductivity (Al) $(\mathrm{W.K^{-1}.m^{-1}})$	150
Thickness of plate (m)	0.01
Aluminum melting point (K)	932

303

304 The performance of a thermocouple depends on the working temperature, and the temperature
305 difference between the hot and cold plates. For this section, modelling strategies employed
306 previously [27–33] have been used.

307 The temperature difference between the hot and the cold plate ($\Delta T = T_h - T_c$) leads to the open
308 circuit voltage $V_{oc} = S(T_m) \cdot \Delta T$ due to the Seebeck effect given by

309 $$S(T_m) = |S_n(T_m)| + |S_p(T_m)|, \quad (12)$$

310 where $S(T_m)$ is the Seebeck coefficient, which depends on the mean temperature between the
311 hot and cold side, T_m . $S_n(T_m)$ and $S_p(T_m)$ are the Seebeck coefficients for the n-type and p-type
312 semiconductors, respectively. The value of $S(T_m)$ can be found in the literature and enables
313 computation of the open circuit voltage:

314 Considering *n* thermocouples assembled in series, the open circuit voltage for the TEG is given
315 by $U_{oc} = n \cdot V_{oc}$.

316 Each thermocouple is made of one n-type and p-type leg with resistivity ρ_n and ρ_p , respectively,
317 which depend on the mean temperature. Therefore, the internal resistance of one thermocouple
318 is:

319 $$R_i = [\rho_n(T_m) + \rho_p(T_m)] \cdot \frac{h_{leg}}{A_{leg}}, \quad (13)$$

320 h_{leg} being the height of the leg (4.9 mm) and A_{leg} its area (2.5 mm * 2.5 mm) only for the case of
321 SiGe based thermocouples. Other thermocouples use a fixed resistance given in their
322 datasheets. The internal resistance for the TEG made of *n* thermocouples assembled in series
323 is:

324 $$R_{i\,TEG} = n \cdot R_i \quad (14)$$

To maximize the power output from the TEG, the load resistance $R_{L\,TEG}$ (the resistance of the electrical system attached to the TEG) has to match the internal resistance, $R_{L\,TEG} = R_{i\,TEG}$. Thus, the load current I_L and voltage U_L are:

$$I_L = \frac{U_{oc}}{R_{i\,TEG} + R_{L\,TEG}} \qquad (15)$$

$$U_L = U_{oc} - I_L \cdot R_{i\,TEG} \qquad (16)$$

The output power provided by the TEG module is given by $P_{\text{elec}} = U_L \cdot I_L$.

Although the TEG module produces electricity out of the TM (hot source), one must consider that it also absorbs heat from it. This absorbed heat reduces the temperature of the TM during the polar night, which in turn decreases the temperature gradient across the TEG needed for electricity production. This negative retroactive effect has been considered in our study.

To obtain the relationships for the absorbed and rejected power in the TEG, three heat transfer mechanisms inside the thermocouple shall be considered. The Fourier process based on the material conductivity κ and the temperature difference ΔT between each side; the Joule heat dissipated due to current flows I_L and internal electrical resistance R_i ; and the Peltier cooling/heat effect which is the phenomenon of heat absorption or dissipation at the junction of two dissimilar materials when an electrical current flow through this junction [28]. The heat absorbed or rejected based on the Peltier effect is given by $S(T) \cdot I_L \cdot T_{h\,\text{or}\,c}$. The combination of these three mechanisms for n thermocouples, gives the power absorbed at the hot side, and the power rejected at the cold side:

$$P_{abs} = n \cdot \left\{ -\frac{1}{2} \cdot R_i \cdot I_L^2 + S(T_m) \cdot I_L \cdot T_h + \kappa \cdot \Delta T \right\} \qquad (17)$$

$$P_{rej} = n \cdot \left\{ \frac{1}{2} \cdot R_i \cdot I_L^2 + S(T_m) \cdot I_L \cdot T_c + \kappa \cdot \Delta T \right\} \qquad (18)$$

The material thermal conductivity is often missing in TEG datasheet. However, it can be extracted from $\kappa = \frac{S(T_m)^2}{R_i \cdot Z}$, where $Z = \frac{Z_T(T_{hot})}{T_{hot}}$, Z_T being the figure of merit. Therefore, the following

parameters are required to compute all outputs: T_{hot}, T_{cold}, n, $Z_T(T_{hot})$, R_i or $R_i(T_m)$ and S or S (T_m).

In the present case, three thermoelectric materials (Bi_2Te_3 [29], PbTe/TAGS [32], and SiGe [33]) have been considered and their properties are summarized in Table A.1 of Appendix A. The model of the TEG was implemented as a MATLAB function.

The TEG function was validated with the performance reported in the literature. The error in the simulated power output with respect to the datasheet is less than 2.5% for Bi_2Te_3 and PbTe/TAGS. For SiGe-based TEG, the simulated power output is within the uncertainty range presented in [33].

4.4 Modelling the cooling subsystem

The Cooling Subsystem (CS) works as follows: a cold plate absorbs the heat rejected by the thermoelectric generator, and the heat is evacuated to the radiator. As for the hot side, the chosen material is Aluminum. The temperature of the cold plate is computed as the temperature of the radiator assuming an ideal transfer of the TEG rejected heat. The chosen initial temperature in order to simulate the polar day is 250 K.

The radiator receives heat from the TEG and dissipates it towards the cold deep space. Thus, it is thermally coupled with space and the Moon's surface. Each contribution depends on the radiator geometry and orientation (view factors), the topography of the site, and the temperature profile of the lunar soil at that place. An ideal location for the radiator at the South Pole would be a permanent or long shadowed region. In this case, the radiator will achieve maximum performance due to the low environment temperature.

The radiator is assumed to be made of Aluminum. A coating surface is considered to maximize emitted heat flux, ε_{rad} , and minimize absorbed solar flux, α_{rad}. At beginning-of-life, common values for white epoxy materials are $\varepsilon_{rad} = 0.9$ and $\alpha_{rad} = 0.25$ [34]. However, due to solar high-energy radiation (UV), most of the coatings age over time and, degraded sizing values were used: $\varepsilon_{rad} = 0.8$ and $\alpha_{rad} = 0.4$. These values do not account for lunar dust depositing onto the radiator which could affect its overall emissivity and absorptivity.

The evolution of the temperature of the radiator is given by:

$$\frac{dT_{rad}}{dt} = \frac{1}{m_{rad}\, c_{p_{rad}}} \cdot \left(P_{rej} + P_{sun} - P_{radiator \to space} - P_{radiator \to moon}\right), \qquad (19)$$

where m_{rad} is the mass of the radiator, $c_{p_{rad}}$ is the specific heat of Aluminum, P_{sun} is the incoming power from the solar irradiance, $P_{radiator \to space}$ is the radiative power losses towards space, and $P_{radiator \to moon}$ is the net power transferred to the Moon surface. This latter contribution is assumed to be negligible, due to temperature equilibrium between the radiator placed directly on the fluff insulating regolith, and the possibility of carefully selection of the coating material. P_{sun} is given by:

$$P_{sun} = A_{rad} \alpha_{rad} \phi_{sun}, \qquad (20)$$

A_{rad} being the area of the radiator, α_{rad} the absorptivity of the coating, and ϕ_{sun} the direct sun irradiance. On the poles the maximum sun elevation is about 1.54° which would lead to an irradiance of $37\ \mathrm{W.m^{-2}}$. However, direct solar irradiance has been taken $100\ \mathrm{W.m^{-2}}$ as a worst-case value. This is to account for non-flatness of the local terrain which could cause the maximum sun elevation with respect to the radiator plane to be higher than expected at the poles. The radiator size needed is about 10 m^2.

The radiative power loss to space is given by:

$$P_{radiator \to space} = f_{rs} A_{rad} \varepsilon_{rad} \sigma \left({T_{rad}}^4 - {T_{space}}^4\right), \qquad (21)$$

where f_{rs} is the view factor considered equal to one (radiator placed horizontally on the lunar surface).

The change in temperature of the radiator (and thus the cold side) in a simulation time step Δt is finally given by:

$$\Delta T_{cold} = \Delta T_{rad} = \frac{1}{m_{rad}\, c_{p_{rad}}} \cdot \left(P_{rej} + P_{sun} - P_{radiator \to space}\right) \cdot \Delta t \qquad (22)$$

5. Results and Discussion

5.1 Performances optimizations and results

For the proposed TES/TEG concept, the main performance drivers have been identified through a fractional factorial design. Preliminary simulations have shown that the temperature experienced by the TEG at the hot sink is close to 410 K at the end of the polar night. Given this specific temperature differential (240 K) between the hot and cold plates and the cold plate temperature at the end of the darkness period (170 K), Bi_2Te_3 shows an efficiency (9.3%) higher than PbTe/TAGS (<9%) or SiGe (<3%). Bi_2Te_3 is the most obvious suitable material unless further materials are implemented in the model. It is worth mentioning that in the case of Bi_2Te_3, temperature-dependent properties were not available from the datasheet. However, due to the modularity of our model, it can be added in the future for better accuracy of results.

The influence of seven factors on the performance of the system was analyzed. The following four factors showed a significant influence:

- The power output of a TES/TEG unit at the end of a polar night is improved when the height of the TM it is set at 0.65 m rather than at 1 m.
- The ability of the cover cap to mitigate radiative losses. The model gave much better performance with a TM emissivity reduced by a factor 50 than with a TM emissivity reduced only by a factor 10 during the polar night.
- The achievable cold temperature plays an important role: 170 K at the cold side instead of 200 K significantly increases the power output.
- The presence of a thermal beam inside the TM substantially improved the system performance. Optimization of the dimension and location of this beam for better performances is left for future works. It is currently a preliminary design which gives a good compromise between performances improvement and mass of the thermal beam.

Other studied factors which had a negligible influence are:

- The surface occupied by the TEG (0.2 or 0.3 m^2), which impacts the absorbed heat flux.

- The depth at which the TEG is placed in the TM (0.2 or 0.3 m from the TM surface).
- The number of thermocouples per TEG (50 or 80).

Thanks to the identification of the main performance drivers, an ultimate simulation is performed which leads to the best performance of the system in the considered scenario. The numerical simulations reproduced the behavior of the system during 150 hours of concentrated sunlight followed by 66 hours of darkness. The results are presented in Fig. 4 and Fig. 5.

A steady temperature is reached at the end of the polar day (Figs. 4a and 5a). The top of the thermal mass reaches 1000 K while the bottom temperature stays at 600 K. This persistent gradient is explained by the relatively low thermal conductivity of sintered regolith, the heat absorbed by the TEG and the losses by conduction in native regolith.

At the end of the 66 hours of polar night, the temperature in the TM is more homogeneous and decreases to about 420 K (Figs. 4b and 5a). The coldest spots are the regions near the TEGs (Fig. 4b), since each TEG plate absorbs between 200 W and 400 W from the TM (Fig. 5d).

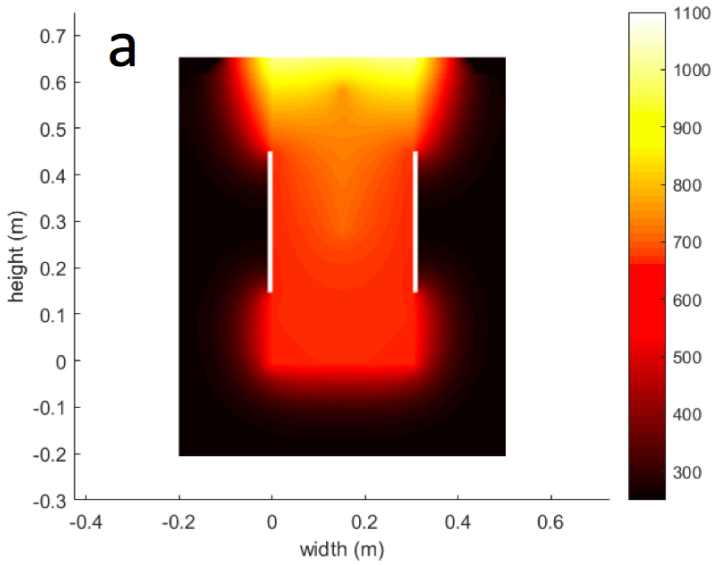

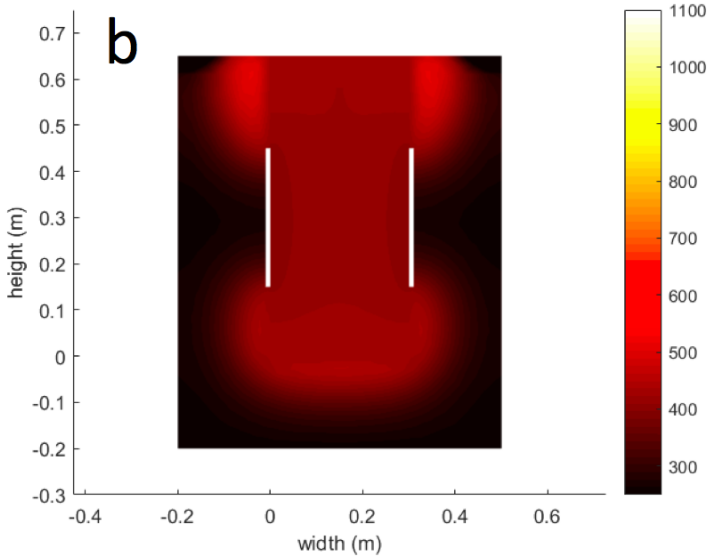

439

440 **Figure 4:** Temperature profile (K) of the thermal mass (a) after 150 hours of applied
441 concentrated sunlight (b) after 66 hours of radiative losses in the polar night. White rectangles
442 are the TEG modules.

443 The temperature difference achieved between the hot and the cold plates ranges from 240 K to
444 400 K (Fig. 5b). The peak observed after sunset is due to the sudden decrease of the cold plate
445 temperature. This peak in turn results in a peak in the power output (Fig. 5c), the heat flow
446 through each TEG element (Fig. 5d), and the efficiency of the TEG elements (Fig. 5e). The
447 efficiency of the TEG is within the range of expected values for thermoelectric materials (8 % to
448 11 %).

449 Similar to the TM temperature, the power output reaches a constant value during the polar day
450 at approximately 42 W per TEG (Fig. 5c) and sharply decreases during the polar night. At the
451 end of the darkness period, only 18 W are produced per TEG. Hence, the proposed concept
452 which includes two TEG plates provides a minimum of 36 W at any time during the 66 hours of
453 darkness considered.

454 Fig. 5f shows the number of required elements to provide 10 kW to a surface payload with a
455 very conservative 50% margin (accounting for a safety factor and low TRL technology). At the
456 end of the polar night, approximately 420 elements are needed to provide the required power.

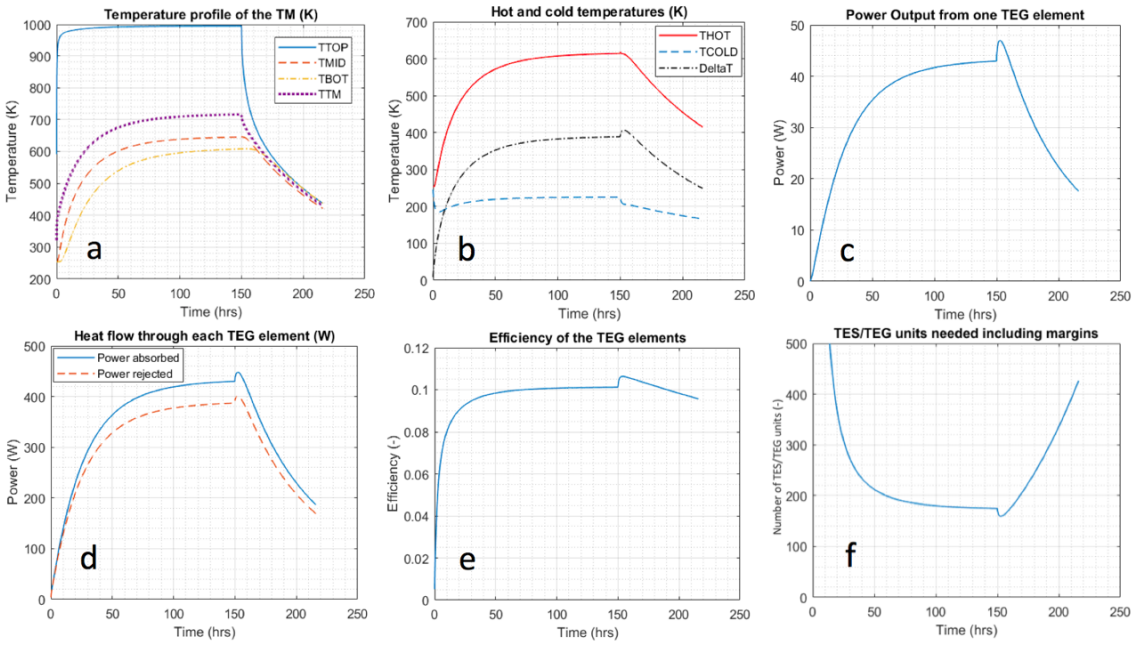

457

458 **Figure 5:** (a) temperature profile of the TM at the top (TTOP), mid-height (TMID), bottom
459 (TBOT), and mean value (TTM). (b) Temperature difference between the hot and cold plates (c)
460 Power output of one TEG (d) Power absorbed and rejected at the hot and cold plate,
461 respectively. (e) Efficiency of the TEG elements. f) Number of TES/TEG elements needed
462 including 50% to comply with 10 kW power requirement of a Moon base.

463 **5.2 Trade-off Analysis**

464 Trade-off analyses are frequently used to evaluate the potential of various alternatives, in order
465 to support a decision-making process. In the present case, the philosophy is to use it as a tool
466 to assess objectively the potential of our scenario concept with respect to more conventional
467 approaches. The analyzed systems are:

468 1) The TES/TEG system modelled in the present study.

469 2) A combination of solar panels and rechargeable batteries. This is the current approach used
470 on-board the ISS and by most of space missions in the vicinity of the Earth.

471 3) A combination of solar panels and regenerative fuel cells. This is a promising system since
472 fuel cells benefit from significant space heritage.

4) Fission Surface Power. An important advantage of this system is the continuous power production irrespective of the irradiance conditions, with a relatively compact system.

The trade-off analysis was performed considering the following criteria:

- **Mass of the power system:** Launch costs represent a significant part of any mission, and therefore a low-mass system is desirable given a fixed power requirement.
- **Global specific power**: Power output per unit of mass for the system. It is denoted as "global" since it is computed considering the global energy system mass (i.e. production units, storage mean, resources extracted from the Moon, structural elements, etc.). This criterion enables to assess the "compactness" of the system on the Moon.
- **Space heritage**: A space-proven technology is more likely to be used than a technology which requires years and considerable investment in research and technology development. The space heritage can be assessed using the technology readiness level scale (TRL)**.**
- **System complexity:** All characteristics being equal, a simple system is a better solution than a complex system. Indeed, knowledge acquisition is easier, and more confidence is placed during operations and maintenance. Furthermore, the end users would be able to interact easily, modify and adapt the system depending on real on-site situations.
- **Installation efforts:** This criterion aims to quantify the level of efforts that needs to be placed into the installation in the energy system before being operational. Some systems may be ready to use, mechanically deployable, or "plug & play". Some others might require robotic assisted installation, extensive ISRU, or extra-vehicular activities (EVAs) on the Moon surface.
- **Operations:** This criterion encompasses daily work required for astronauts, robots, ground control center, but also maintenance of the system. Safety issues due to hazardous components will also complicate operations, maintenance or work nearby the system.
- **Scalability:** The power system not only aims to provide electrical power to the primary habitat, but might be used for surface robots, pressurized rovers, EVA systems.

Moreover, new infrastructures will be progressively implemented and added to the main base in the “Moon Village”. Thus, it is important for a power system to be versatile, to interface with all of these elements, and to be scalable for increasing or decreasing power demand.

- **Lifespan:** For a long-duration program, the lifetime of the considered system should be high. Although no missions are yet fully planned, it is assumed that the return of humans to the Moon’s surface will be permanent, as it was for the Low-Earth Orbit. With unknown duration set, it is better to promote long lifespan systems, to account for permanent presence from program starting date.
- **Potential benefits for Earth systems:** Innovation and challenges encountered by engineers, scientist and astronauts often lead to advances beyond the limits of our technologies potentially leading to spin-off Earth applications.
- **End-Of-Life:** This criterion aims to assess potential constraints due to end-of-life management of the system, decommissioning, and recyclability for other uses.

Each technology has been assessed with respect to the criteria. The detailed scoring rules, the criteria weights, their evaluation and justification are available in Appendix B. Table 3 shows the synthesis trade-off matrix.

Table 3: Synthesis of the trade-off matrix for comparison of the performances of four energy production and storage systems at the rim of the Shackleton Crater (66 hours of polar night): Good (++); Medium (+); Bad (-); Very Bad (x). Baseline requirement is a power demand of 10kW.

Criteria/Systems	Solar Panels & Batteries	Solar Panels & Fuel Cells	Fission Surface	Thermal Energy Storage
Mass to be delivered from Earth	-	+	+ +	x
Specific Power	-	+	+ +	x
Space Heritage	+ +	+ +	+	-
System Complexity	+ +	-	x	+
Installation Efforts on the Moon	+ +	+	+	x
Operations	+ +	+ +	-	+ +
Scalability (up and down)	+ +	+	+	-
Lifespan	+	+	-	+ +
Potential benefit for Earth energy	+	+ +	-	+
End-of-life (recyclability, constraints?)	-	-	x	+
Total Figure of Merit	**85**	**80**	**46**	**28**

According to the results of the trade-off analysis, the use of a TES/TEG system to power the lunar base for 66 hours of darkness is not favorable with respect to other approaches. This negative result assessment is reinforced by the fact that the results were obtained in the best-case scenario, which is the unique spot of the Moon suspected to provide polar night as short as 66 hours [2]. This implies that such architecture would be much less able in harsher conditions. The main drawbacks in comparison with the alternative “Solar panels and Batteries” and “Solar panels and Regenerative Fuel Cells” are:

- Need of significant mass to be transported from Earth although ISRU activities take place (reflectors, Fresnel lens, TEG, aluminum plates, radiators). We estimated the delivered mass for one TES/TEG unit at 198 kg (see mass budget in appendix table B.2). Since it is computed that 420 units are required, the mass to be delivered to the Moon surface is about 82 tons for 10 kW of power demand. This is greater than for all other alternatives by almost a factor 5.
- Huge efforts necessary for installation. The total mass of regolith to be sintered on the Moon has been estimated to be about 245 metric tons. In addition, all the enabling systems to deploy the TES/TEG power architecture on the Moon were not considered

(comprising excavation, sintering, and connections of more than 420 TES/TEG units) which would add in reality considerable labor, costs, complexity and energy consumption for sintering.

- Lack of space heritage.

Despite the poor performance of the TES/TEG concept for the considered power requirement (10 kW), the outcome of this study is valuable because it shows that ISRU-based processes are not systematically advantageous against scenarios of Earth supplies.

6. Conclusions and future work

An integrated model of the TES/TEG concept has been presented in this paper. One major feature is the ability of the model to account for temperature dependent properties of the TM and TEG which was not the case in previous studies. The proposed system employs a TM of $1\ \mathrm{m} \times 0.3\ \mathrm{m} \times 0.65\ \mathrm{m}$ and Bi_2Te_3 thermoelectric generators. The system has been optimized to reach 36 W at the end of the 66 hours of the considered polar night 2 m above the surface at the rim of the Shackleton crater.

A trade-off analysis has been conducted in order to compare the TES/TEG concept with other architectures (solar arrays and batteries, solar arrays and regenerative fuel cells, fission surface power). The trade-off ranked the proposed TES/TEG system with thermoelectricity generation as the least appropriate alternative.

This result obtained under the best-condition scenario is valuable in a period of enthusiasm towards ISRU. It shows that processes exploiting extraterrestrial materials instead of Earth supplies are not systematically attractive. In actual fact, detailed analyses are required to verify if it has merit. Likewise, the ineffectiveness of thermoelectricity suggested in this specific case, should not preclude the use of thermal energy storage in a different architecture, or for other usages and scenarios.

Therefore, a number of follow-on considerations could also be studied which would open up the idea of ISRU TES systems in a more practical application:

- Integration of more efficient heat engines (TEGs with higher efficiencies, or a Stirling engine, which has a conversion efficiency of 25 to 30%) [9].
- Changing the location of the TEG on the TM appears very promising. We suggest replacing the TM cover cap by a TEG array which can be moved to be in contact with the top surface of the TM. During the polar day, the TEG array is not in contact with the surface that accumulates solar energy. During the darkness period, the TEG array is retracted and placed in contact with this hot surface. The advantage is that this surface is the hottest spot at the beginning of the nighttime, it prevents radiative losses and the need of a cover cap. This approach also reduces the need of a cooling system (including potential loop heat pipes) since the cold side area radiates directly the wasted energy towards deep space. The main drawback is the need for another power system during the polar day but this can be easily overcome with high-efficiency photovoltaic panels.
- Use of a TES/TEG only as a reliable power backup system instead of a primary power supply system, or only for thermal management purposes (thermal energy reservoir as part of a thermal Wadi concept) [15,35].
- Modelling of a single large power Thermal Energy Storage system: a 10-kW engine, and a large-scale TM with internal fluid loop heat pipes to enhance heat transfer for storage and release [9].

References

[1] ESA, Moon Village, (2016). http://www.esa.int/About_Us/Ministerial_Council_2016/Moon_Village (accessed April 15, 2019).

[2] P. Gläser, J. Oberst, G.A. Neumann, E. Mazarico, E.J. Speyerer, M.S. Robinson, Illumination conditions at the lunar poles: Implications for future exploration, Planet. Space Sci. (2017) 1–9. doi:10.1016/j.pss.2017.07.006.

[3] D. Rapp, Use of Extraterrestrial Resources for Human Space Missions to Moon or Mars, Springer, 2013. doi:10.1007/978-3-642-32762-9.

[4] D. Shrunk, B. Sharpe, B. Cooper, M. Thangavelu, THE MOON: Resources, Future Development, and Settlement, Second, Praxis Publishing Ltd, 2008.

[5] D.A. Paige, M.C. Foote, B.T. Greenhagen, J.T. Schofield, S. Calcutt, A.R. Vasavada, D.J. Preston, F.W. Taylor, C.C. Allen, K.J. Snook, B.M. Jakosky, B.C. Murrary, L.A. Soderblom, B. Jau, S. Loring, J. Bulharowski, N.E. Bowles, I.R. Thomas, M.T. Sullivan, C. Avis, E.M. De Jong, W. Hartford, D.J. McClesse, The Lunar Reconnaissance Orbiter Diviner Lunar Radiometer Experiment, Sp. Sci Rev. (2010) 125–160. doi:10.1007/s11214-009-9529-2.

[6] A. Colaprete, P. Schultz, J. Heldmann, D. Wooden, M. Shirley, K. Ennico, B. Hermalyn, W. Marshall, A. Ricco, R.C. Elphic, D. Goldstein, D. Summy, G.D. Bart, E. Asphaug, D. Korycansky, D. Landis, L. Sollitt, Detection of Water in the LCROSS Ejecta Plume, Science (80-.). 330 (6003) (2010) 463–468. doi:10.1126/science.1186986.

[7] NASA/GSFC, Multi-temporal illumination map of the lunar south pole, (2010). https://www.nasa.gov/mission_pages/LRO/multimedia/gallery/121510pole.html (accessed April 15, 2019).

[8] R. Balasubramaniam, R. Wegeng, S. Gokoglu, N. Suzuki, K. Sacksteder, Analysis of Solar-Heated Thermal Wadis to Support Extended-Duration Lunar Exploration, in: AIAA-

615 2009-1339, 2010.

616 [9] B. Climent, O. Torroba, R. González-cinca, N. Ramachandran, M.D. Griffin, Heat
617 storage and electricity generation in the Moon during the lunar night, Acta Astronaut. 93
618 (2014) 352–358. doi:10.1016/j.actaastro.2013.07.024.

619 [10] ESA, Buidling a Lunar Base With 3D Printing, (2010).
620 http://www.esa.int/Our_Activities/Space_Engineering_Technology/Building_a_lunar_bas
621 e_with_3D_printing (accessed April 15, 2019).

622 [11] P. Fleith, In-Situ Approaches for Thermal Energy Storage and Thermoelectricity
623 Generation on the Moon: Modelling and Simulation, Master's Thesis - European
624 Astronaut Centre (ESA) / ISAE-SUPAERO, 2017.

625 [12] R.H. Turner, Space power system utilizing Fresnel lenses for solar power and also
626 thermal energy storage, in: Eighteenth Intersoc. Energy Convers. Eng. Conf., American
627 Institute of Chemical Engineers, Orlando (FL), 1983: pp. 971–976.

628 [13] A.V. Lozano, Development of a Lunar Regolith Thermal Energy Storage Model for a
629 Lunar Outpost, Master's Thesis - European Astronaut Centre (ESA) / Université Paul
630 Sabatier Toulouse III, 2016.

631 [14] A. Colozza, Analysis of Lunar Regolith Thermal Energy Storage, 1991.

632 [15] H.L. Jones, J.P. Thornton, R. Balasubramaniam, S.A. Gokoglu, K.R. Sacksteder, W.L.
633 Whittaker, Enabling Long-Duration Lunar Equatorial Operations With Thermal Wadi
634 Infrastructure, 2011.
635 https://ntrs.nasa.gov/archive/nasa/casi.ntrs.nasa.gov/20110007929.pdf.

636 [16] P.L. Córdoba, Thermal Energy Storage Demonstrator, Master's Thesis - European
637 Astronaut Centre (ESA) / UPC, 2017.

638 [17] A.R. Vasavada, J.L. Bandfield, B.T. Greenhagen, P.O. Hayne, M.A. Siegler, J. Williams,
639 D.A. Paige, Lunar equatorial surface temperatures and regolith properties from the
640 Diviner Lunar Radiometer Experiment, J. Geophys. Res. 117 (2012) 1–12.

641 doi:10.1029/2011JE003987.

642 [18] M.T. Mellon, B.M. Jakosky, H.H. Kieffer, P.R. Christensen, High-Resolution Thermal
643 Inertia Mapping from the Mars Global Surveyor Thermal Emission Spectrometer, Icarus.
644 148 (2000) 437–455. doi:10.1006/icar.2000.6503.

645 [19] G. Heiken, D. Vaniman, B.M. French, Lunar sourcenook: A user's guide to the Moon,
646 (1991).

647 [20] A.R. Vasavada, D.A. Paige, S.E. Wood, Near-Surface Temperatures on Mercury and the
648 Moon and the Stability of Polar Ice Deposits, Icarus. 141 (1999) 179–193.

649 [21] B.S. Hemingway, R.A. Robie, W.H. Wilson, Specific heats of lunar soils, basalt, and
650 breccias from the Apollo 14, 15, and 16 landing sites, between 90 and 350°K, in: Lunar
651 Sci. Conf. 4th, SAO/NASA Astrophysics Data System (ADS), n.d.: pp. 2481–2487.

652 [22] M.G. Langseth, S.J. Keihm, K. Peters, Revised lunar heat-flow values, in: Lunar Sci.
653 Conf. 7th, Houston, Texas, SAO/NASA Astrophysics Data System (ADS), 1976: pp.
654 3143–3171.
655 http://articles.adsabs.harvard.edu//full/1976LPSC....7.3143L/0003169.000.html.

656 [23] D.L. Mitchell, I. De Pater, Microwave Imaging of Mercury's Thermal Emission at
657 Wavelengths from 0.3 to 20.5 cm, Icarus. (1994) 2–32.

658 [24] C.J. Cremers, Thermophysical Properties of Apollo 12 Fines, Icarus. 18 (1973) 294–303.

659 [25] R. Morrel, Thermal conductivities, Tables Phys. Chem. Constants. (n.d.).
660 http://www.kayelaby.npl.co.uk/general_physics/2_3/2_3_7.html (accessed February 3,
661 2018).

662 [26] W. Callister, D. Rethwisch, Materials science and engineering: an introduction, in: Mater.
663 Sci. Eng., 2007: pp. 266–267. doi:10.1016/0025-5416(87)90343-0.

664 [27] H. Alam, S. Ramakrishna, A review on the enhancement of figure of merit from bulk to
665 nano-thermoelectric materials, Nano Energy. 2 (2012) 190–212.

666 doi:10.1016/j.nanoen.2012.10.005.

667 [28] H. Tsai, J. Lin, Model Building and Simulation of Thermoelectric Module Using Matlab /
668 Simulink, J. Electron. Mater. 39 (2009) 2105–2111. doi:10.1007/s11664-009-0994-x.

669 [29] Termo-Gen AB, Datasheet Bismuth telluride TEG Modules (TEP1- 12656-0.6), (2006).
670 http://www.termo-gen.com/pdf/TEG_modules_Bi2Te3.pdf (accessed April 15, 2019).

671 [30] E. Kanimba, Z. Tian, Modeling of a Thermoelectric Generator Device, in: InTechOpen,
672 2016: pp. 461–479.

673 [31] D. Tatarinov, M. Koppers, G. Bastian, D. Schramm, Modeling of a Thermoelectric
674 Generator for Thermal Energy Regeneration in Automobiles, J. Electron. Mater. 42
675 (2013) 2274–2281. doi:10.1007/s11664-013-2642-8.

676 [32] TEC Solidstate Power Generators, Datasheet for High Efficiency Pb/TAGS TEG
677 Modules (PBTAGS-200:009A10), (n.d.). http://tecteg.com/wp-
678 content/uploads/2016/05/PBTAGS-200.009A10.pdf (accessed April 15, 2019).

679 [33] K. Romanjek, S. Vesin, L. Aixala, T. Baffie, J. Dufourcq, High-Performance Silicon –
680 Germanium-Based Thermoelectric Modules for Gas Exhaust Energy Scavenging, J.
681 Electron. Mater. 44 (2015) 2192–2202. doi:10.1007/s11664-015-3761-1.

682 [34] C. Nicollier, Particle Flux in the Earth Environment, 2019.

683 [35] R. Balasubramaniam, R. Wegeng, S. Gokoglu, N. Suzuki, K. Sacksteder, Extended-
684 Duration Lunar Exploration, 2010.
685 https://ntrs.nasa.gov/archive/nasa/casi.ntrs.nasa.gov/20100015637.pdf.

686

Appendix A – Thermoelectric Materials Properties

Table A.1: Thermoelectric generator properties for the three selected materials Bi2Te3: [29], PbTe/TAGS [32], and SiGe [33]. The data obtained from the datasheet for Bi_2Te_3 and PbTe/TAGS are constant but from commercially available TEGs. Data on SiGe taken from [33]. The resulting equations given for SiGe were obtained through polynomial fitting trend lines for these sources.

Properties of TC	**Value / function of temperature**
Bi_2Te_3 [29]	
Temperature range (K)	200 to 500
Internal resistance of a TC $(\mathrm{m\Omega})$	9.75
Seebeck coefficient $(\mu \mathrm{V.K^{-1}})$	372.2
Figure of Merit $(-)$	0.86
PbTe/TAGS [32]	
Temperature range (K)	300 to 700
Internal resistance of a TC $(\mathrm{m\Omega})$	11.4
Seebeck coefficient $(\mu \mathrm{V.K^{-1}})$	280
Figure of Merit $(-)$	0.85
SiGe [33]	
Temperature range (K)	500 to 1000
n-type resistivity $(\Omega.\mathrm{m})$	$-4.73 \times 10^{-14} \cdot T^3 + 7.86 \times 10^{-11} \cdot T^2 - 1.96 \times 10^{-8} \cdot T + 2.54 \times 10^{-}$
p-type resistivity $(\Omega.\mathrm{m})$	$6.51 \times 10^{-12} \cdot T^2 + 9.75 \times 10^{-9} \cdot T + 7.4 \times 10^{-6}$
Seebeck coefficient $(\mathrm{V.K^{-1}})$	$-2 \times 10^{-10} \cdot T^2 + 6.39 \times 10^{-7} \cdot T + 1.06 \times 10^{-4}$
Figure of Merit $(-)$	$Z_{T_{n-type}}(T_{hot}) = 4.286 \times 10^{-7} \cdot {T_{hot}}^2 + 7.589 \times 10^{-4} \cdot T_{hot} - 0.1720$

Appendix B – Trade-off analysis

The details of the trade-off analysis performed to compare four systems to satisfy the power demand during the polar night at the specified location are presented here. Table B.1 shows the cooperative method that has been used to assign the weights to each criterion. Table B.2 shows the scoring rules for each criterion. Table B.3 shows the systematic approach to determine the figure of merit of each approach with respect to the proposed criteria.

Table B.1 Trade-off weights were averaged after independent consultation of 4 researchers within the team (anonymously identified by A, B, C and D). The highest is the weight, the most it will affect the total scores.

Criterion/Researcher preferred weights	**A**	**B**	**C**	**D**	**Average Weight**
Mass of the Power System	5	5	3	4.5	**4.4**
Global Specific Power	1.5	1	4	1.5	**2.0**
Space Heritage	2	2	4	3.5	**2.9**
System Complexity	2.5	4	4	1	**2.9**
Installation Efforts	2.5	3	5	2.5	**3.3**
Operations	3	3	3	1.5	**2.6**
Scalability	2	1	3	4	**2.5**
Lifespan	3	4	5	4.75	**4.2**
Potential benefit for Earth	0.5	1	1	0.25	**0.7**
End-of-life	1	2	1	0.25	**1.1**

707 **Table B.2** Trade-off scoring rules. Each system scores +5; +3; +0 or -3 points per criterion

708 depending on the scoring rules. The total score is calculated with a weighted average.

Criteria / Scoring (points)		**Good (+5)**	**Medium (+3)**	**Bad (0)**	**Very Bad (-3)**
Power System Mass	[kg]	< 10000	10000 - 20000	20000 - 30000	> 30000
Global Specific Power	[$W.kg^{-1}$]	> 2	2-1	1-0.25	< 0.25
Space Heritage	TRL	6 or +	4-5	2-3	1
System Complexity	[see index]	1 or less	2-3	4-5	> 5
Installation Efforts	[see index]	0	1-2	3-4	5
Operations	[see index]	1 or less	2-3	4	> 4
Scalability	[-]	5W - 100kW	High-power only	low-power only	no
Lifespan	[years]	> 15	10-15	4-10	< 4y
Potential benefit for Earth	[-]	Strong	Possible	Unlikely	No
End-of-life	[see index]	3	2	1	0

709

710

711 **Table B.3** Criteria assessment and justifications

Power System Mass

All masses were estimated using the internal ESA mass budget tool. The given figures include a safety factor of 1.5 to applied on the energy storage requirement.

1. Solar Arrays & Batteries: **17867 kg (bad)**
    i. 222 kg of solar arrays
    ii. 14667 kg of batteries (Li-ion)
    iii. 2978 kg for harness, structure, and power control and distribution unit
2. Solar Arrays & Regenerative Fuel Cells: **6507 kg (Medium)**
    i. 1256 kg of solar arrays
    ii. 211 kg of electrolyzers
    iii. 40 kg of fuel cells
    iv. 4750 kg of hydrogen and oxygen tank dry mass
    v. 250 kg of power control and distribution unit.
    vi. (optional 1600 kg of water that could be brought from Earth or mined on the moon)
3. Fission Surface Power: **3700 kg (Good)**
    No storage required
4. Thermal Energy Storage: **83205 kg (Very Bad)**
    i. 420 TES/TEG units required
    ii. 2 Hot sink plate per unit: 3.24 kg
    iii. Thermal beam per unit: 8.1 kg
    iv. 5m^2 radiator per unit: 33.75 kg
    v. 21m^2 Fresnel lens per unit: 84 kg
    vi. 30 m^2 reflectors per unit: 30 kg
    vii. Heat Pipes per unit: 6 kg
    viii. Holding Structure, sun-trackers, Power control distribution unit (optimistic 20%): 33 kg
    ix. Total is 198 kg per unit

Global Specific Power

1. Solar Arrays & Batteries: **0.56 W/kg (Bad)**
2. Solar Arrays & Regenerative Fuel Cells: **1.54 W/kg (Medium)**
3. Fission Surface Power: **2.7 W/kg (Good)**
4. Thermal Energy Storage: **0.12 W/kg (Very Bad)**

Space Heritage

1. Solar Arrays & Batteries: **TRL 9 (Good)**
2. Solar Arrays & Regenerative Fuel Cells: **TRL 6+ (Good)**
3. Fission Surface Power: **TRL 4 (Medium)**
4. Thermal Energy Storage: **TRL 2-3 (Bad)**

System Complexity (high index is bad)

The scoring rules refers to a system complexity index computed by addition of the points recommended if applicability of the following statement:

- Slow-motion or occasionally moving parts? (+1)
- High-velocity moving parts? (+3)
- Non-hazardous, easy to store working fluid? (+1)
- One hazardous, difficult to store working fluid? (+2)
- Multiple working fluids? (+3)
- Considerable vibrations? (+1)
- Tendency to be unstable, uncontrollable (+1)

1. Solar Arrays & Batteries: **complexity index = 1 (Good)**
2. Solar Arrays & Regenerative Fuel Cells: **complexity index = 4 (Bad)**
3. Fission Surface Power: **complexity index = 8 (Very Bad)**
4. Thermal Energy Storage: **complexity index = 2 (Medium)**

Installation Efforts on the Moon (high index is bad)

The scoring rules refers to a installation index computed by addition of the points recommended if applicability of the following statement:

- A couple of hours of work, almost plug and play and can be done robotically (+0)

- Humans required on-site for installation, only a few hours of work (+1)
- Little ISRU, be can be avoided with extra-mass brought from Earth (+2)
- Significant ISRU required (+3)
- More than 300 manned hours of installation (+3)

1. Solar Arrays & Batteries: **installation index = 0 (Good)**
2. Solar Arrays & Regenerative Fuel Cells: **installation index = 2 (medium)**
3. Fission Surface Power: **installation index = 2 (medium)**

   (A Fission Surface Power plant shall be installed autonomously before the arrival of the crew to minimize risks. It could be assisted by robots, or self-deployable. The fission reaction can be started only when the reactor is on-site. There are not significant installation efforts to be made, because it shall be made autonomously or robotically.)
4. Thermal Energy Storage: **complexity index = 5 (Very Bad)**

   (In order to install such system with 420 units to satisfy the 10kW power, we estimate the mass to be sintered to be 246 metric tons. This is considerable and would require specialized rover, and already utilize tremendous amount of energy in the building phase.)

Operations (high index is bad)

The scoring rules refers to an operations index computed by addition of the points recommended if applicability of the following statement:

- Any serious safety issue, for transportation, launch or work around the base? (+2)
- Weekly maintenance estimated > 2hrs? (+1)
- Needs of Astronauts daily intervention > 30min (+2)
- Critical, non-repairable element? (+2)
- Remote monitoring necessary from Earth? (+1)

1. Solar Arrays & Batteries: **operations index = 0 (Good)**
2. Solar Arrays & Regenerative Fuel Cells: **operations index = 1 (Good)**

   (high-pressure systems to be monitored)
3. Fission Surface Power: **operations index = 4 (Bad)**

There is of course safety issue with nuclear power sources, and most of the parts in the core of the system will be neither replaceable nor repairable by astronauts, but this task will be done robotically. Due to its nature, operations performed by astronauts will be minimized if no banned. Mostly, the reactor will be monitored remotely.

4. Thermal Energy Storage: **complexity index = 1 (Good)**

Scalability

1. Solar Arrays & Batteries: **5W – 100kW (Good)**
2. Solar Arrays & Regenerative Fuel Cells: **high-power mostly (Medium)**
3. Fission Surface Power: **high power only (Medium)**
4. Thermal Energy Storage: **low power only (Bad)**

Lifespan

1. Solar Arrays & Batteries: **10 – 15 years (Medium)**

   Lifespan limited by the battery lifetime which represent most of the subsystem mass.
2. Solar Arrays & Regenerative Fuel Cells: **10 years (Medium)**
3. Fission Surface Power: 5 to 10 **(Bad)**
4. Thermal Energy Storage: **> 15 years (Good)**

Potential benefits for Earth systems

1. Solar Arrays & Batteries: **possible (Medium)**
2. Solar Arrays & Regenerative Fuel Cells: **strong (Good)**

   (hydrogen very much regarded as future energy vector)
3. Fission Surface Power: **unlikely (Bad)**
4. Thermal Energy Storage: **possible (Medium)**

End-of-life (high index => good)

The scoring rules refers to an End-of-Life index computed by addition of the points recommended if applicability of the following statement:

- Significant recyclability? (+3)
- Little recyclability? (+2)
- Not recyclable but no EOL constraints? (+1)

- Significant EOL constraints (0)

---

1. Solar Arrays & Batteries: **1 (Bad)**
2. Solar Arrays & Regenerative Fuel Cells: **1(Bad)**
3. Fission Surface Power: **0 (Very Bad)**
4. Thermal Energy Storage: **2 (Medium)**

712

Declaration of interests

 The authors declare that they have no known competing financial interests or personal relationships that could have appeared to influence the work reported in this paper.

☐The authors declare the following financial interests/personal relationships which may be considered as potential competing interests: